Molecular Pharmacology Fast Forward. Published on June 18, 2007 as doi:10.1124/mol.107.038398
This article has not been copyedited and formatted. The final version may differ from this version.

MOL #38398

HUMAN PREGNANE X RECEPTOR ANTAGONISTS AND AGONISTS DEFINE MOLECULAR REQUIREMENTS FOR DIFFERENT BINDING SITES

Sean Ekins, Cheng Chang, Sridhar Mani, Matthew D. Krasowski, Erica J. Reschly, Manisha Iyer, Vladyslav Kholodovych, Ni Ai, William J. Welsh, Michael Sinz, Peter W. Swaan, Rachana Patel and Kenneth Bachmann

ACT LLC, 601 Runnymede Avenue, Jenkintown, PA 19046 and Department of Pharmaceutical Sciences, University of Maryland, 20 Penn Street, Baltimore, MD 21201.

Molecular Pharmacology Fast Forward. Published on June 18, 2007 as DOI: 10.1124/mol.107.038398
This article has not been copyedited and formatted. The final version may differ from this version.

MOL #38398

Running title: PXR antagonist binding site

Corresponding author: Sean Ekins, D.Sc., Senior Vice President, Computational Biology, ACT LLC, 601 Runnymede Avenue, Jenkintown, PA 19046. Phone 215-687-1320; Fax 215-481-0159; Email ekinssean@yahoo.com

Number of Text pages:

Tables:	3 (2 supplemental)
Figures:	4
References:	65
Words in Abstract:	247
Words in Introduction:	1067
Words in Discussion:	2030

The abbreviations used are: LBD, ligand binding domain; QSAR, quantitative structure-activity relationship.

Molecular Pharmacology Fast Forward. Published on June 18, 2007 as DOI: 10.1124/mol.107.038398
This article has not been copyedited and formatted. The final version may differ from this version.

ABSTRACT

The pregnane X receptor (PXR) is an important transcriptional regulator of the expression of xenobiotic metabolism and transporter genes. The receptor is promiscuous binding many structural classes of molecules which act as agonists at the ligand binding domain, triggering up-regulation of genes, increasing the metabolism and excretion of therapeutic agents and causing drug-drug interactions. Recently it has been suggested that human PXR antagonists represent a means to counteract such interactions. Several azoles have been hypothesized to bind the activation function-2 (AF-2) surface on the exterior of PXR when agonists are concurrently bound in the ligand binding domain. In the present study, we have derived novel computational models for PXR agonists using different series of imidazoles, steroids and a set of diverse molecules with experimental PXR agonist binding data. We have additionally defined a novel pharmacophore for the steroidal agonist site. All agonist pharmacophores showed hydrophobic features are predominant. In contrast, a qualitative comparison with the corresponding PXR antagonist pharmacophore models using azoles and biphenyls showed they are smaller and hydrophobic with increased emphasis on hydrogen bonding features. Azole antagonists were docked into a proposed hydrophobic binding pocket on the outer surface at the AF-2 site and fitted comfortably making interactions with key amino acids involved in charge clamping. Combining computational and experimental data for different classes of molecules provided strong evidence for agonists and antagonists binding distinct regions on PXR. These observations bear significant implications for future discovery of molecules that are more selective and potent antagonists.

Molecular Pharmacology Fast Forward. Published on June 18, 2007 as DOI: 10.1124/mol.107.038398
This article has not been copyedited and formatted. The final version may differ from this version.

INTRODUCTION

The human pregnane X receptor, PXR (NR1I2; also known as SXR or PAR) is a transcriptional regulator of the enzyme CYP3A4 (Bertilsson et al., 1998; Blumberg et al., 1998; Kliewer et al., 1998), CYP2B6 (Goodwin et al., 2001), CYP2C9 as well as many other enzymes and transporters such as P-glycoprotein (ABCB1) (Synold et al., 2001) and proteins involved in the transport, metabolism and biosynthesis of bile acids (Staudinger et al., 2001a; Staudinger et al., 2001b). These discoveries have shown how drugs may regulate not only their own metabolism but potentially their efflux too, as demonstrated for paclitaxel (Schuetz and Strom, 2001). Overall, there is an incredibly broad structural diversity in the molecules which bind to human PXR *in vitro* and as yet this has not been summarized extensively in reviews. A small sample of the molecules published and suggested to bind PXR include: bile salts (Krasowski et al., 2005a; Schuetz and Strom, 2001), cholesterol and its metabolites (Sonoda et al., 2005), statins (El-Sankary et al., 2001), endocrine disruptors (Takeshita et al., 2006; Takeshita et al., 2001), synthetic peptide bond mimetics (Mu et al., 2005), anticancer compounds (Mani et al., 2005), herbal components and plant extracts (Ding and Staudinger, 2005; Moore et al., 2000; Mu et al., 2006), carotenoids (Ruhl, 2005; Ruhl et al., 2004), vitamins (Zhou et al., 2004), HIV protease inhibitors (Dussault et al., 2001), calcium channel modulators (Drocourt et al., 2001), steroids (Moore and Kliewer, 2000), plasticizers (Masuyama et al., 2000; Masuyama et al., 2002; Takeshita et al., 2001), pesticides (Coumol et al., 2002; Lemaire et al., 2004), peroxisome proliferator-activated receptor gamma antagonists (Leesnitzer et al., 2002), as well as other diverse xenobiotics and endobiotics (Ekins and Erickson, 2002; Lehmann et al., 1998; Luo et al., 2002; Schuster et al., 2006; Ung et al.,

Molecular Pharmacology Fast Forward. Published on June 18, 2007 as DOI: 10.1124/mol.107.038398
This article has not been copyedited and formatted. The final version may differ from this version.

2007; Waxman, 1999) including agonists for additional nuclear receptors (Xue et al., 2007a).

X-ray crystallography of the ligand binding domain (LBD) of PXR (Watkins et al., 2003a; Watkins et al., 2003b; Watkins et al., 2002; Watkins et al., 2001) suggests it is a large, flexible mostly hydrophobic site with some key polar residues. A recent co-crystal structure indicates 17β-estradiol bridges between the polar residues Ser247 and Arg410 and represents overlapping interactions with the previous crystal structures for more diverse molecules (Xue et al., 2007b). Binding of the coactivator SRC-1 to activation function-2 (AF-2) on the surface of PXR is key for stabilizing the receptor (Watkins et al., 2003a). A recent X-ray crystallographic structure of PXR with the liver X receptor (LXR) agonist T-0901317 was employed to examine potential PXR antagonists that bind in the LBD (Xue et al., 2007a). The authors concluded that due to the flexibility and promiscuity of the LBD identifying such antagonists might be difficult. Known antagonists for PXR include ET-743 (Synold et al., 2001), polychlorinated biphenyls (Tabb et al., 2004) and some azoles (Huang et al., 2007; Takeshita et al., 2002; Wang et al., 2007a). For example, Takeshita showed that ketoconazole disrupted the co-repressor silencing mediator for retinoid and thyroid receptors (SMRT) receptors as well as SRC-1 from binding with PXR (Takeshita et al., 2002). More recently ketoconazole (Huang et al., 2007), fluconazole and enilconazole (Wang et al., 2007a) have been shown to inhibit the activation of PXR in the presence of paclitaxel, while the azoles are themselves weak agonists on their own. Ketoconazole inhibits the PXR-SRC-1 interaction and therefore likely binds the AF-2 site, however it failed to antagonize a double mutant T248E/K277Q PXR which may be due to the synergistic effects of these two residues creating a site for

Molecular Pharmacology Fast Forward. Published on June 18, 2007 as DOI: 10.1124/mol.107.038398
This article has not been copyedited and formatted. The final version may differ from this version.

a lower level coactivator binding than seen in the wild type. These mutations are in the AF-2 binding pocket and not in the ligand binding pocket. Therefore, it is implied that the original residues Lysine and Threonine (which lie in the AF-2 side) must be important for ketoconazole binding and inhibitory interaction (Wang et al., 2007a). This led the authors to speculate that ketoconazole mimics the histidine residue of SRC-1 in interacting at the AF-2 site. The isothiocyanate sulforaphane, a dietary compound found in broccoli, was recently shown to function as a PXR antagonist by displacing ligands from the LBD and inhibiting PXR-coactivator recruitment (Zhou et al., 2007). Importantly, this represents the first naturally occurring human PXR antagonist.

The clinical implications of modulating the transcription of drug metabolizing enzymes and transporters via PXR are therefore important for minimizing drug-drug interactions. In view of the wide array of molecules that bind PXR, our ability to predict potential interactions and adverse drug reactions that may accelerate clearance of drugs and, consequently, diminish efficacy (Zhou et al., 2007) is critical for drug discovery and development, as well as for toxicology assessment. Several predictive computational models for PXR have been developed to define key features of ligands that bind (Bachmann et al., 2004; Ekins and Erickson, 2002; Schuster et al., 2006). Most pharmacophore models feature 4-5 hydrophobic features and at least 1-2 hydrogen bonding moieties. In addition, a statistical quantitative structure activity relationship (QSAR) model using VolSurf descriptors and partial least squares (PLS) was described for 33 PXR ligands which identified hydrogen bond acceptor regions and amide responsive regions, while no test set data were provided (Jacobs, 2004). A second statistical model using a recursive partitioning method has been used with 99 PXR

Molecular Pharmacology Fast Forward. Published on June 18, 2007 as DOI: 10.1124/mol.107.038398
This article has not been copyedited and formatted. The final version may differ from this version.

activators and non-activators to predict the probability of aprepitant, L-742694, 4-hydroxytamoxifen and artemisinin binding to PXR (Ekins et al., 2006). Additional models based on machine learning methods using a set of PXR activators and non-activators (Ung et al., 2007) displayed overall prediction accuracies between 72 and ~80% while an external test set of known activators had a similar level of accuracy. To date we are not aware of the application of ligand-based or protein-based methods for modeling PXR antagonists.

The novel aims of the current study were to use a combination of *in vitro* data and computational methods (pharmacophores, Comparative Molecular Field Analysis (CoMFA)) for PXR agonists and antagonists to define the important features and locations for binding, to answer the question of whether the PXR antagonists assessed bind in the LBD or at the AF-2 site. Finally we have used a structure-based docking method to position azole antagonists and further support our ligand-based approaches to rationalize the *in vitro* data and previously published mutagenesis study (Wang et al., 2007a). This research represents the first combined computational modeling of PXR antagonists and different series of PXR agonists.

Molecular Pharmacology Fast Forward. Published on June 18, 2007 as DOI: 10.1124/mol.107.038398
This article has not been copyedited and formatted. The final version may differ from this version.

MATERIALS AND METHODS

Reagents and Plasmids. The DPX-2® cell line was a gift from Puracyp Inc., (Carlsbad, CA). The corresponding dosing and culturing media were purchased from the same. The construction of the HepG2 (human liver) cells stably expressing human SLC10A1, a transporter that can take up conjugated bile salts has been reported before in detail (Krasowski et al., 2005a). Human PXR was expressed as a full-length protein and CYP3A4-PXRE-Luc, which contains promoter elements from CYP3A4 recognized by the PXR DNA-binding domain, was used as the reporter construct. The plasmids for human PXR, human SLCO1A2, CYP3A4-PXRE-Luc, and empty vectors pSG5 were generously provided by S.A. Kliewer, J.T. Moore, and L.B. Moore (GlaxoSmithKline, Research Triangle Park, NC). Clotrimazole, mifepristone, androstenol, pregnenolone 16α-carbonitrile, rifampicin and sterile filtered dimethyl sulfoxide (DMSO) were purchased from Sigma-Aldrich (St. Louis, MO). 5α-Petromyzonol and allocholic acid were obtained from Toronto Research Chemicals (North York, Ontario, Canada). All other steroids and bile salts were purchased from Steraloids (Newport, RI). Tissue culture petri dishes were acquired from VWR International (West Chester, PA). Opaque, tissue culture-treated, sterile white ninety-six plates were purchased from Perkin-Elmer Inc (Boston, MA). Clear-bottom, tissue culture treated sterile white ninety-six well plates were purchased from Fisher Scientific (Pittsburgh, PA). The Steady-Glo Luciferase Assay System to measure induction, the CellTiter-Glo Luminescent Cell Viability Assay System and all other laboratory equipment required for cell culture were purchased from Fisher Scientific.

Molecular Pharmacology Fast Forward. Published on June 18, 2007 as DOI: 10.1124/mol.107.038398
This article has not been copyedited and formatted. The final version may differ from this version.

Reporter gene assay with DPX-2® cells: The protocols describing the cell culture techniques and standard operating procedures for the reporter gene assay, obtained from Puracyp Inc., were accurately followed. The tissue culture protocols were performed in the sterile laminar flow hood. All incubations were carried out at 37º C and 5% CO_2.

The DPX-2® cells were obtained frozen in liquid nitrogen. Following successful cell plating and generation of a viable cell line, media was aspirated and replaced every two days until the cells reached 70-80% confluency. The medium was aspirated and cells rinsed with 5 mL PBS. PBS was replaced with 2 mL trypsin/EDTA and incubated for 5 minutes. 2 mL medium was added and the entire mixture was transferred to a 15 mL centrifuge tube. Cells were pelleted at 500 rpm for 3 minutes, and re-suspended in 5 mL culturing medium. The cell density was determined using 0.4% trypan blue in sterile filtered PBS and a Brightline Hemocytometer. The cells were diluted to achieve the desired concentration. 100 µL of cell suspension corresponding to 30,000 cells was added to each well of a 96-well plate, using a 12 channel pipettor and special wide bore pipette tips. The plates were incubated overnight. Drug stock solutions (10 mM for each compound) were prepared in dimethyl sulfoxide (DMSO) and diluted directly into the dosing medium. The final DMSO concentration of 0.1% was maintained in all dilutions. DPX-2® cells plated in 96-well dishes were treated with selected inducers by replacing the medium in each well with 150 µL of media containing an appropriate concentration of inducer or DMSO control; each condition was repeated in quadruplicate. Subsequently each plate examining the test compounds was also, treated with 10 µM rifampicin, mifepristone and androstenol as known comparators of varying effectiveness (potent,

Molecular Pharmacology Fast Forward. Published on June 18, 2007 as DOI: 10.1124/mol.107.038398
This article has not been copyedited and formatted. The final version may differ from this version.

moderate or weak) for PXR activation. Test articles included clotrimazole and eight novel azole compounds: CDD3501, CDD3508, CDD3530, CDD3532, CDD3536, CDD3538, CDD3540 and CDD3543. Apart from rifampicin which was tested at 0.5, 1, 5, 10, 15, 20, 25 and 30 μM all other compounds were diluted to 0.1, 0.5, 1, 5, 10, 15 and 20 μM from the stock solution. After a 24-hour treatment, cell medium containing test compound or DMSO was aspirated from the wells and frozen for future analysis. 100 μL of room temperature Dulbeccos' PBS (DPBS) was added to each well. DPBS was added as it contains calcium and magnesium ions necessary for the luminescence assay. Promega SteadyGlo Luciferase reagent and Cell TiterGlo Viability reagent were prepared as per manufacturer's protocol by combining the substrate buffer solution with the lyophilized substrate solution. 100 μL of the induction/viability reagent was added to the designated plates and mixed thoroughly by pipetting up and down five times. Induction and viability assays were conducted in separate plates as it was found that the strong luminescence associated with the viability assay interfered with the luminescence obtained with induction. The plates were placed away from light to allow for dark adaptation. They were sealed with self-adhesive clear plastic sheets and luminescence was quantified on the TopCount NXT. The TopCount was normalized and adjusted to detect luminescence in each well for 30 seconds.

Reporter gene assay with HepG2 cells: PXR activation in the HepG2 human liver cell line was determined by a luciferase-based reporter assay as previously described (Krasowski et al., 2005b). The basic methodology for the luciferase reporter assays in 96-well format was as follows. HepG2-SLC10A1 cells were grown in modified Eagle's medium-α containing 10% fetal bovine serum and 1% penicillin/streptomycin

Molecular Pharmacology Fast Forward. Published on June 18, 2007 as DOI: 10.1124/mol.107.038398
This article has not been copyedited and formatted. The final version may differ from this version.

(Invitrogen, Carlsbad, CA, USA) at 37ºC in 5% CO_2. On day 1, cells were seeded onto 96-well white opaque plates at 30,000 cells/well. On day 2, the medium was exchanged, and cells were transfected using calcium phosphate precipitation. For experiments involving human PXR, 25 ng/well of CYP3A4-PXRE-Luc reporter, 2.7 ng/well human PXR (in pSG5 plasmid), and 20 ng/well pSV-β-galactosidase (Promega, Madison, WI, USA) were co-transfected. For experiments involving sulfated steroids or bile salts, human SLCO1A2 was co-transfected at 10 ng/well to facilitate uptake of sulfated compounds. On day 3, the cells were washed with Hanks' buffered salt solution (Invitrogen) and then exposed to media containing the test molecules or vehicle to be tested. The medium utilized charcoal-dextran-treated fetal bovine serum (Hyclone, Logan, UT, USA) to reduce background activation. Cells were washed once with Hanks' buffered salt solution and then lysed with 150 μL lysis buffer (Reporter Lysis Buffer, Promega). Separate aliquots were taken for measurement of β-galactosidase activity (Promega) and luciferase activity (Steady-Glo, Promega). Each drug concentration was performed at least in quadruplicate and repeated in separate experiments for a total of at least three times. Data are expressed as mean ± SD. Complete concentration-response data were collected for all compounds with at least 8 concentrations per compounds tested. Some of the data for the bile salts has been previously reported (Krasowski et al., 2005a).

To test for cytotoxicity, two assays that have been well-validated in HepG2 cells were used: 3-(4,5-dimethylthiazol-2-yl)-2,5-diphenyltetrazolium bromide (MTT) reduction and alamar blue reduction. Both assays sensitively measure the ability of viable cells to metabolize the parent compound to a metabolite that can be detected by

Molecular Pharmacology Fast Forward. Published on June 18, 2007 as DOI: 10.1124/mol.107.038398
This article has not been copyedited and formatted. The final version may differ from this version.

spectrophotometry or fluorometry (Hamid et al., 2004). HepG2 cells were seeded at a density of 20,000 cells/well (100 μL per well) into clear 96-well microplates (for the MTT assay) or black, opaque 96-well plates (for the alamar blue assay) and grown for 24 hours. The next day, 100 μL solutions of drug concentrations or vehicle controls in cell growth medium at twice the intended final concentration were added to the cells (final volume 200 μL). The cells were again incubated for 24 hr. For the MTT assays, MTT (*In vitro* toxicology assay kit, MTT-based; Sigma, St. Louis, MO, USA) was dissolved at 5 mg/mL in warm cell growth medium. 20 μL of this solution was added to the cells (total volume 220 μL), and the plates incubated for another 4 hrs. After incubation, the supernatant was removed and 50 μL of solubilization buffer provided in the Sigma kit with 0.5% DMSO was added. DMSO was added to ensure total solubility of the formazan crystals. Plates were shaken for 2 min, and the absorbance recorded at 590 nm. The percent viability was expressed as absorbance in the presence of test compound as a percentage of that in the vehicle control (with subtraction of background absorbance).

For the alamar blue assays, alamar blue stock solution (Biosource International; Camarillo, CA) was diluted 1:1 with cell growth medium and 50 μL of this was added to each well, yielding a final concentration of 10% alamar blue (total volume 250 μL). The plates were exposed to an excitation wavelength of 530 nm, and the emission at 590 nm was recorded to determine whether any of the test drug concentrations fluoresce at the emission wavelength. Plates were returned to the incubator for 5 hr and the fluorescence was measured again. The percent viability was expressed as fluorescence counts in the presence of test compound as a percentage of that in the vehicle control (with subtraction of background fluorescence). Drug concentrations that cause > 30% loss of cell viability

Molecular Pharmacology Fast Forward. Published on June 18, 2007 as DOI: 10.1124/mol.107.038398
This article has not been copyedited and formatted. The final version may differ from this version.

in the MTT assay or > 15% loss of cell viability in the alamar blue assay were not used in the determination of concentration-response curves for activation of PXRs.

Data generation for PXR antagonists. The assays used to generate the effect of azole and imidazole antagonists for PXR have been previously described in detail and the reader is referred to these (Huang et al., 2007; Mani et al., 2005; Wang et al., 2007a).

Statistical Analyses. Dose response curves were plotted for each imidazole compound tested, including the positive controls using Kaleidagraph Software (Synergy Software, Reading, PA). The equation for the logistic dose response curve was represented by the rearranged form of the Hill's Equation:

$$E = 1 + \left[\frac{C^n (E_{max} - 1)}{C^n + C_{50}^n} \right] \qquad \text{eq.1}$$

Dose response curves were additionally plotted using the E_{max} model equation:

$$E = \left(\frac{[C] * E_{max}}{[C] + EC_{50}} \right) \qquad \text{eq.2}$$

For the E_{max} model, curves were forced to plateau for the 3 controls; rifampicin, mifepristone and androstenol, by artificially setting set an E_{max} at the average of the highest consistent fold-induction values.

Fold-induction was calculated as the ratio of the luminescence obtained with treatment of test compound compared to treatment with 0.1% DMSO (control). The control was added to each 96-well plate to account for any inter-plate variability. The raw data was appropriately labeled. Of the four replicates performed for each assay point, any one replicate was discarded if it deviated significantly (greater than one fold) from the other three results. The average of the DMSO replicates was calculated and this represented the negative control. The average of each dilution of each control and test

Molecular Pharmacology Fast Forward. Published on June 18, 2007 as DOI: 10.1124/mol.107.038398
This article has not been copyedited and formatted. The final version may differ from this version.

article was calculated along with the average of the media alone replicates (no DMSO). The media alone average represented the background control and helped to determine if the DMSO had deteriorated. The average was used for comparison to DMSO: if it lay within 10% of the DMSO reading, it was discarded. Fold induction for each dilution of controls and test articles was calculated by dividing the average of the test results by the average of the negative control. For clotrimazole, final induction data were represented by the average of 3 distinct assays. Figures for each data point were normalized to viability. For viability, results were expressed as fold induction in viable cells. The number of viable cells was determined as a ratio to DMSO treated cells.

For the steroidal compounds concentration response curves were fitted using Kaleidagraph. The relative efficacies (ε) for each compound are the maximal response of the test ligand divided by the maximal response obtained with 10 μM rifampicin. Compounds with $\varepsilon < 0.05$ were considered 'inactive'. All comparisons to maximal activators were done within the same microplate.

***In silico* modeling: Catalyst™.** The computational molecular modeling studies were carried out using Catalyst version 4.9 (Accelrys, San Diego, CA) running on a Silicon Graphics (Palo Alto, CA) Octane workstation. Pharmacophore models attempt to describe the arrangement of key features that are important for biological activity. Briefly, the Catalyst models were employed to generate hypotheses. After sketching the molecules in Catalyst, the 3-D molecular structures were produced using up to 255 conformers with the best conformer generation method, allowing a maximum energy difference of 20 kcal/mol. A Hypogen PXR agonist pharmacophore was generated with Catalyst™ using the steroidal agonist data derived from HepG2 cells in this study and

Molecular Pharmacology Fast Forward. Published on June 18, 2007 as DOI: 10.1124/mol.107.038398
This article has not been copyedited and formatted. The final version may differ from this version.

recently published data for 31 diverse molecules with EC_{50} values (Sinz et al., 2006) (Supplemental Table 1). Ten hypotheses were generated using these conformers for each of the molecules and the EC_{50} values, after selection of the following features: hydrophobic, hydrogen bond acceptor, hydrogen bond donor and ring aromatic features. After assessing all ten generated hypotheses, the hypothesis with lowest energy cost was selected for further analysis as this possessed features representative of all the hypotheses and had the lowest total cost. The quality of the structure activity correlation between the estimated and observed activity values was estimated by means of an *r* value.

When the set of molecules was too small for a Hypogen model, HIPHOP was used to align the molecules, which is independent of biological activity. Catalyst™ was used to generate a common features (HIPHOP) (Clement and Mehl, 2000) pharmacophore. Up to 255 conformers were generated for each molecule with the best conformer generation method allowing a maximum energy of 20 kcal/mol. A HIPHOP pharmacophore for the imidazole PXR agonists (Table 1, Figure 1) was generated from alignment of all 8 CDD compounds and clotrimazole. All molecules were aligned to the clotrimazole structure. For the equipotent (~10 μM) PXR antagonists enilconazole, ketoconazole and fluconazole (Huang et al., 2007) a HIPHOP pharmacophore was generated. In this case the template molecule was ketoconazole, to which the other two molecules were aligned. Molecules were then aligned using hydrophobic, hydrogen bond acceptor, hydrogen bond donor and ring aromatic features.

In silico modeling: CoMFA. Comparative Molecular Field Analysis (CoMFA, Tripos, St Louis, MO) is a widely applied QSAR method that attempts to explain the gradual changes in observed biologic properties by evaluating the electrostatic

Molecular Pharmacology Fast Forward. Published on June 18, 2007 as DOI: 10.1124/mol.107.038398
This article has not been copyedited and formatted. The final version may differ from this version.

(Coulombic interactions) and steric (van der Waals interactions) fields at regularly spaced grid points surrounding a set of mutually aligned structures (Cramer et al., 1988).

Of all the aspects required for CoMFA modeling, correctly aligned structures is most essential to ensure successful and meaningful model results, hence this method is generally used with homologous structural series. For the imidazole agonist data set, the clotrimazole structure was first sketched in Sybyl using standard bond distances and lengths. Following initial optimization, systematic search was performed allowing all flexible bonds to rotate with 10 degree increments. The conformation with lowest energy from systematic search was further optimized using energy minimization. The final optimized structure was used as a scaffold for the generation and optimization of all other imidazole derivatives. All structures were aligned according to the central carbon atom and the four anchoring points of the phenyl groups.

Separately, nineteen differently substituted polychlorinated biphenyls (PCB) that were previously suggested as human PXR antagonists (Tabb et al., 2004) were also analyzed using CoMFA (Supplemental Table 2). The molecules were similarly sketched and optimized in Sybyl. The backbone alignment was straightforward since all structures possess identical rigid backbone structures. Care was taken to ensure that the chlorinated site on each molecule maximally overlapped each other.

In all cases electrostatic and steric interaction fields were calculated using an sp3 hybridized carbon probe atom (+1 charge at 1.52 Å van der Waals radius) on a 2.0 Å spaced lattice, which extends beyond the dimensions of each structure by 4.0 Å in all directions. A cutoff of 30 kcal/mol ensures that no extreme energy terms will distort the final model. The indicator fields and hydrogen bond fields generated by the advanced

Molecular Pharmacology Fast Forward. Published on June 18, 2007 as DOI: 10.1124/mol.107.038398
This article has not been copyedited and formatted. The final version may differ from this version.

CoMFA module were also included in the analysis. To eliminate excessive noise, all electrostatic interaction energies below 1.0 kcal/mol and steric interaction energies below 10.0 kcal/ mol were set to zero. PLS was used to correlate the field descriptors with biologic activities. CoMFA descriptors were used as independent variables, whereas the dependent variable (biologic descriptor) used in these studies was -LogEC_{50} (imidazole agonists) and –LogK_i (PCB data). The predictive value of the models was evaluated first using leave one out (LOO) cross-validation. The cross-validated standard coefficient, q^2, was calculated as follows:

$$q^2 = 1 - \frac{\sum_{Y} (Y_{predicted} - Y_{observed})^2}{\sum_{Y} (Y_{observed} - Y_{mean})^2} \qquad \text{eq.3}$$

where $Y_{predicted}$, $Y_{observed}$, and Y_{mean} are the predicted, observed, and mean values of the target property (-LogEC_{50} or –LogKi), respectively. $\Sigma(Y_{predicted}-Y_{observed})^2$ is the predictive error sum of squares (PRESS). The standard error of the cross-validated predictions is represented as *press*, whereas the root mean squares of the conventional (non-cross-validated) analysis is known as *s*. The model with the optimum number of PLS components, corresponding to the lowest PRESS value was selected to derive the final PLS regression model. In addition to the q^2, the conventional correlation coefficient r^2 and its standard error were also calculated. A plot of predicted versus experimental activity was used to identify potential outliers. The process was repeated until no further improvements in q^2 or no outliers could be identified. Results from alternative descriptor fields were compared, and the model with the highest q^2 was selected for later analysis. A contour plot of standard coefficients enclosing the highest 20 % value was created for each model (except the electrostatic positive favorable interaction, blue contour, for the

Molecular Pharmacology Fast Forward. Published on June 18, 2007 as DOI: 10.1124/mol.107.038398
This article has not been copyedited and formatted. The final version may differ from this version.

imidazole agonist model, where the top 10% values were plotted for clarity). The contours of the steric map are shown in yellow and green, while the contours of the electrostatic map are shown in red and blue. Greater activities (lower EC_{50} values for PXR agonists and lower K_i values for PXR antagonists) are correlated with less bulk near yellow areas, whereas more bulk is tolerated near green areas. More negative charge is preferred near red regions, while more positive charge is needed near blue regions.

In silico modeling: docking antagonists to the crystal structure using GOLD. Protein preparation for GOLD docking (Jones et al., 1997) was done in Sybyl 7.2 (Tripos Inc, St.Louis, MO). From the Protein Databank entry 1NRL and the larger fragment of chain A, Ser192-Gly433, was chosen for a protein site preparation. Water molecules, salt ions, ligands and co-receptor fragments were deleted. Only hydrogen position energy optimization was performed after addition of hydrogen atoms and assigning of the AMBER 02 force field charges to a protein. The resulting protein was saved in Tripos mol2 format and used later as a docking site in GOLD.

The 1NRL chain A was used for rigid docking in which the protein was fixed and only flexibility was allowed for ligands. Each ligand was set to dock 20 times. An automatic cavity detection around Glu427, approximately x 1.345, y 20.932, z 18.464 was performed on chain A with a 15Å radius to make sure all atoms of the SRC-1 binding groove were covered. This was termed site 1. GOLD also explores adjunct regions for docking. A second docking site (site 2) was defined around the atom on the protruding tip of SRC-1. x 3.582, y 16.389, z 21.454 with a radius of 5 Å only.

Molecular Pharmacology Fast Forward. Published on June 18, 2007 as DOI: 10.1124/mol.107.038398
This article has not been copyedited and formatted. The final version may differ from this version.

RESULTS

Imidazole PXR agonist pharmacophore. The first published PXR pharmacophore (Ekins and Erickson, 2002) generated with EC_{50} data for 12 agonists had previously been used to predict human PXR interactions for 3 imidazoles that were shown to increase apoA1 and HDL-C in rodents (Bachmann et al., 2004) (Table 1). These predictions suggested the molecules were likely to be agonists. The experimental data from this current study confirm that all 3 molecules are indeed low μM agonists of human PXR in DPX-2 cells (Table 1). In addition, a luciferase based reporter assay was performed using HepG2 cells as described previously (Zhu et al., 2004) using an 11 point dose response curve from 2.5-50μM and this also demonstrated that 4 of the novel imidazoles and clotrimazole were low μM agonists of human PXR (Table 2). These same molecules also behaved as antagonists as they were also competitive inhibitors of rifampicin binding, indicative that they were likely binding in the LBD. The imidazoles were found not to be cytotoxic in this reporter assay (data not shown).

As the computational predictions for the novel imidazoles binding to human PXR as agonists diverged from the experimental data in terms of the ranking, this necessitated the generation of a separate pharmacophore for the 9 imidazoles used in this study which were all found to have low μM affinity, but with a range of E_{max} values (with some molecules with comparable efficacy to rifampicin). As there was not the required 3 log unit variation in biological activity necessary for Hypogen pharmacophore generation, we opted to align the compounds using common features. The common features HIPHOP pharmacophore consisted of 3 ring aromatic (hydrophobes) and a single hydrogen bond acceptor (Figure 2A). The mapping of these molecules is similar to the previously

Molecular Pharmacology Fast Forward. Published on June 18, 2007 as DOI: 10.1124/mol.107.038398
This article has not been copyedited and formatted. The final version may differ from this version.

observed alignment to 3 of the 4 hydrophobes in the original PXR pharmacophore from which our initial predictions were derived (Bachmann et al., 2004).

Imidazole PXR agonist CoMFA analysis. A highly consistent and predictive PXR agonist model was developed after removing CCD3508 as an outlier. The LOO cross-validated r^2 (q^2) is 0.527 with a PRESS value of 0.24 using five principle components. PC=5). The CoMFA model revealed that contributions were greater from Steric (59 %) interactions than from Electrostatic (41 %) interactions. As shown in Figure 2B, multiple red contours covering the lower benzene group illustrate the favorable substitution of halogen atoms on this ring, thus introducing more negative charge. This explains the higher affinity of clotrimazole, CDD3538 and CDD 3532. The blue contour over the meta position of benzene group indicates substitution with a more negative charge at this position is not favorable for PXR activation, exemplified by the weaker agonist CDD3530 (EC_{50} value: 3.05 μM). The blue contour over the para position of the left ring also indicates that a negative charge at this position is not favorable, while the red contour over the para position of the right ring indicates the favorable substitution of chlorine at this position for PXR activation. These two different correlations may reflect the affinities of CDD3540 (1.72 μM) and CDD3543 (1.44 μM).

Steroidal PXR agonist pharmacophore. The PXR activation data for 30 steroidal molecules include data for nine bile salts which were part of a previous study that compared PXR ligand activation across animal species (Krasowski et al., 2005a). The steroidal ligands possessed a wide EC_{50} range (0.8-104 μM with 9 inactives, Table 3) that was used to derive a Catalyst Hypogen model with an observed versus predicted correlation r = 0.75. The difference between the total cost of the model and the null cost

Molecular Pharmacology Fast Forward. Published on June 18, 2007 as DOI: 10.1124/mol.107.038398
This article has not been copyedited and formatted. The final version may differ from this version.

can be used as an additional indicator of model significance. In this case the total cost = 182.175 compared with null total cost = 248.114 represents an acceptable cost difference compared with previously published Catalyst models (Ekins and Erickson, 2002). The pharmacophore possessed one hydrogen bond acceptor (green) and 4 hydrophobes (cyan, Figure 2C). Aligned to this pharmacophore are the two most active compounds 5α-androstan-3β-ol (red) and lithocholic acid acetate (gray) showing the mapping to these features.

Diverse PXR agonist pharmacophore. The 31 diverse published molecules with EC_{50} data (range 0.04-39 μM) resulted in a Catalyst Hypogen model with an observed versus predicted correlation r = 0.855. However, the total cost = 133.5 compared with the null cost 135.7 does not represent a significant difference in this case. This model consists of two hydrophobes, one hydrogen bond acceptor and one hydrogen bond donor (Figure 2D).

Biphenyl PXR antagonist CoMFA. The iterative analysis during the CoMFA model generation process identified 2,2´,3,3´,4,4´,6-Hepta-chlorobiphenyl (CB), 2,2´,4,4´,5,5´-Hexa-CB, and 2,2´,3,4,4´,5,5´,6-Octa-CB as outliers and excluded them from the final result. The final antagonist model has a similar predictive power as the imidazole agonist CoMFA model, with a q^2 of 0.573 and PRESS of 0.377 using five principle components (PC=5). Both steric and electrostatic interactions contributed to the final model (53% and 47%, respectively). The CoMFA coefficient contour map aligned with the most potent compound 2,2´,3,3´,4,4´,6,6´-Octa-CB is shown in Figure 3A. This is dominated by red contours surrounding both phenyl rings and reflects the favorable chlorine substitutions on both rings. The presence of a blue contour over the 5 position of

the left phenyl ring is the result of absence of a chlorine atom at this position among the most active antagonists.

Azole PXR antagonist Pharmacophore. Enilconazole and fluconazole were aligned to ketoconazole using HIPHOP as they are all suggested to possess similar antagonist activity with PXR (Wang et al., 2007a). The resulting pharmacophore contained two hydrogen bond acceptor features, a hydrophobe and a ring aromatic (hydrophobic) feature (Figure 3B).

Docking of azole antagonists. The results from GOLD docking the 3 azoles in PXR are shown in Figures 4A and 4B. We identified 2 separate locations on either side of Lys277 and in both cases, binding of azoles would interfere with SRC-1 binding in the AF-2 site. The GOLD docking scores for binding at site 1 with enilconazole (43.07), fluconazole (44.46), and ketoconazole (58.41), are higher than at site two with enilconazole (39.13), fluconazole (36.27), and ketoconazole (50.68). The higher score represents a higher predicted affinity for the protein. It was noted that the alignment of ketoconazole to the other two azoles may not be optimal at site 1 (not shown), as they do not seem to be overlapping as one would expect based on their similar antagonist activity (Huang et al., 2007). In contrast, at site 2 the azoles overlap in a manner similar to the Catalyst antagonist pharmacophore (Figure 3B). The site 2 is predominantly hydrophobic. It consists of 15 amino acids. Lys252, Ile255, Lys259, Pro423, Leu424, Glu427 and Leu428 form one side of the groove, and are responsible for accommodation of the diclorophenyl group of ketoconazole. Phe264, Ile269, Glu270, Gln272, Ile273, Ser274 and Leu276 are on the other side of the binding pocket and contribute to the interaction with the azole ring and other heterocyclic groups of the ketaconazole. Lys277 most

Molecular Pharmacology Fast Forward. Published on June 18, 2007 as DOI: 10.1124/mol.107.038398
This article has not been copyedited and formatted. The final version may differ from this version.

likely serves as a “charge clamp” for interaction between the co-activator SRC1 (His687) and PXR, and probably plays a significant role on the initial phase of accommodating azoles in the binding groove of PXR.

Molecular Pharmacology Fast Forward. Published on June 18, 2007 as DOI: 10.1124/mol.107.038398
This article has not been copyedited and formatted. The final version may differ from this version.

DISCUSSION

Qualitative computational comparisons of PXR agonist and antagonist models.

There have been attempts to model PXR agonists using computational methods such as pharmacophores (Bachmann et al., 2004; Ekins and Erickson, 2002; Ekins et al., 2002; Schuster et al., 2006), QSAR (Ekins et al., 2006; Jacobs, 2004; Ung et al., 2007), and homology modeling with molecular dynamics (Wang et al., 2006). These in general made use of data from different experimental groups and did not computationally model PXR antagonism, focus on limited structural types for agonists or assess potential binding sites using such methods. From the various PXR agonist pharmacophores and computational models developed in this study using data from our own laboratories and that published elsewhere (Sinz et al., 2006; Tabb et al., 2004), a consensus emerges that agonists - whether imidazole, steroidal or more diverse structures - are required to fit to multiple hydrophobic features and one hydrogen bond acceptor. For example the imidazole pharmacophore contains 3 hydrophobic ring aromatic features (Figure 2A) and the CoMFA model for imidazole agonists shows a larger contribution of steric versus electrostatic fields (Figure 2B), which is in agreement with the role of hydrophobic interactions for agonists. We have also identified a novel PXR agonist steroidal pharmacophore which contains 4 hydrophobes (Figure 2C) while the diverse molecule pharmacophore contains 2 hydrophobic features (Figure 2D). All of these pharmacophores additionally possess one hydrogen bond acceptor. These results are generally in close accord with the previous PXR agonist pharmacophores (Ekins and Erickson, 2002; Schuster et al., 2006) and crystal structures. In particular the steroidal pharmacophore contains most of the features recently reported with the crystal structure

Molecular Pharmacology Fast Forward. Published on June 18, 2007 as DOI: 10.1124/mol.107.038398
This article has not been copyedited and formatted. The final version may differ from this version.

using 17β-estradiol, indicating one of the two hydrogen bond acceptors, as well as the hydrophobic interactions of the A and B rings (Xue et al., 2007b). The training set for this model also contains 17β-estradiol with an EC_{50} of 16 μM, close to that previously reported in the X-ray crystallography study (20 μM), however it should be noted that the most active compound 5α-Androstan-3β-ol with an EC_{50} value of 0.8 μM has a single hydrogen bond acceptor feature, and therefore both hydrogen bonds in the crystal structure may note be necessary for other steroidal ligands to bind PXR. It should also be noted that the more diverse molecule pharmacophore contains an additional hydrogen bond donor feature but does not possess optimal cost difference values and requires further evaluation. In addition, although previous pharmacophore models have suggested multiple hydrogen bond acceptors (Schuster et al., 2006) a role for a hydrogen bond donor has not been noted (Ekins and Erickson, 2002; Schuster et al., 2006). This would suggest that the two most active molecules in this diverse molecule pharmacophore, SR12813 and hyperforin which both have a single hydroxyl functional group, are aligning their ring features. The hydroxyl on SR12813 was shown to form a π-stacking interaction with Trp299 in the 1NRL crystal structure (Watkins et al., 2003a), providing direct evidence of an important hydrogen bonding interaction that was missed previously when the same two molecules were superimposed (Schuster et al., 2006). An additional observation from this study is the dependence of the resulting agonist pharmacophore on the types of molecules used in the training set, indicative that there may be numerous potential models that partially overlap.

In contrast, the PXR antagonist CoMFA model based on biphenyls appears to have a lower steric and higher electrostatic contribution than those of the imidazole

Molecular Pharmacology Fast Forward. Published on June 18, 2007 as DOI: 10.1124/mol.107.038398
This article has not been copyedited and formatted. The final version may differ from this version.

agonist CoMFA model. The antagonist model is also noticeably smaller (Figure 3A). It has previously been suggested that the substitution patterns that maximize antagonism maximize hydrophobic features on rings in a square-square pattern (Tabb et al., 2004). The azole antagonist HIPHOP pharmacophore (Figure 3B) suggests 2 hydrogen bond acceptor features, a hydrophobic and a ring aromatic (hydrophobic) feature are in common across the three molecules. This seems to indicate a balance between hydrophobic and hydrogen bonding features, which is in agreement with the proportions of steric and electrostatic fields from the biphenyl CoMFA model. As the PXR agonist and antagonist pharmacophores developed in this study are subtly different in their requirement for hydrophobic and hydrogen bonding features, this provides further evidence for likely different binding sites in PXR .

Azoles such as ketoconazole are widely known to interact with many cytochrome P450s as the imidazole ring interacts with the heme. It is also appreciated that there is a difference in the interaction of fluconazole and ketoconazole with CYP51. This may be due to the additional hydrophobic interactions between ketoconazole and CYP51 having a K_d of 8 μM, while the smaller fluconazole is less active with a K_d of 120 μM (Matsuura et al., 2005). In contrast, both of these compounds are suggested as equipotent antagonists of PXR (Huang et al., 2007; Wang et al., 2007a) which may indicate the whole of the ketoconazole structure is unnecessary for antagonist activity. The HIPHOP pharmacophore for the 3 azole PXR antagonists confirms this in two ways. Firstly no pharmacophore features are mapped beyond and including the piperazine ring of ketoconazole. Secondly, antagonist the azole pharmacophore is substantially different from a recently published Hypogen pharmacophore for 26 azole and non azole human

Molecular Pharmacology Fast Forward. Published on June 18, 2007 as DOI: 10.1124/mol.107.038398
This article has not been copyedited and formatted. The final version may differ from this version.

CYP51 inhibitors which possessed 3 hydrophobic features and one hydrogen bond acceptor (Ekins et al., 2007), also suggesting it may be possible to separate the PXR antagonism from P450 inhibition activities.

Docking provides insight into PXR antagonist binding

In order to further rationalize the possible fit of the azole antagonists in PXR we have used an automated docking method called GOLD (Jones et al., 1997) which maintains the protein as rigid and flexibly docks the azole antagonists onto the outer surface of PXR. Definitive experimental mutagenesis data has shown ketoconazole docks in the AF-2 binding pocket and not in the ligand binding pocket (Wang et al., 2007a). Although it has been suggested the azole ring could fit in the vicinity of the SRC-1 histidine which interacts with Lys277 (Wang et al., 2007a), no alignment of ketoconazole has previously been shown. The results in this present study suggest two different binding sites within close proximity to the region where SRC-1 binds the AF-2 site and in particular Lys277, on the outer surface of PXR. The scoring algorithm used with this method indicates that ketoconazole should have a slightly higher affinity than the other 2 azoles. We have selected one of the sites (site 2, Figure 4A) as being more realistic based on the docking of the three azoles in this site. This binding site overlaps with the well known coactivator binding site (AF-2 region) in PXR, which shares similar hydrophobic features common across the nuclear receptor family. The AF-2 region in the nuclear receptor LBD has been shown to form a hydrophobic groove to accommodate the LXXLL motifs (L=Leucine, X=any amino acid residue) or nuclear receptor boxes of p160 coactivators, as demonstrated by the recently solved co-crystal structures of nuclear receptor LBDs and LXXLL motif fragment complexes (Bledsoe et al., 2002; Warnmark

et al., 2002). The leucines of SRC-1 interacting with PXR are 690, 693 and 694. The docking study indicated that ketoconazole occupied two of the three subsites of this motif corresponding to Leu690 and Leu694. We also observed that azoles did not fill the site of Leu693. Thus to achieve optimal antagonistic activity the molecule should be able to cover all three leucine subsites, indicating that the azole affinity can be improved by rational structural design. The interactions between the PXR AF-2 region and its coactivators are essential to its transcriptional activation in the cells. We speculate that the three mentioned azole compounds occupy the AF-2 region and compete for binding with the PXR coactivator in a similar way, therefore disrupting this key protein-protein interaction essential for PXR activation. Previously, a structural homology model and molecular dynamics simulations have been used to assess the interaction of the co-repressor SMRT which was assumed to overlap with the coactivator site of PXR (Wang et al., 2006). Interactions were identified with Lys259, Pro423, Glu427 and Glu270 which were also identified in the current study for the antagonist ketoconazole.

The docking of ketoconazole further indicates that the whole of the molecule may not be important for interaction with PXR as the piperazine ring is solvent exposed and protruded out of the binding groove (Figure 4B) in agreement with the antagonist pharmacophore described above. As the proposed antagonist binding sites are within range of Lys277 they would be affected if this residue changed as has been demonstrated with the double mutant at the 277 and 248 positions (Wang et al., 2007a). It is not known if the double mutant also prevents antagonism by the other two smaller azoles. We are now in a position to use the various computational models to suggest amino acid modifications and further test our different models.

Molecular Pharmacology Fast Forward. Published on June 18, 2007 as DOI: 10.1124/mol.107.038398
This article has not been copyedited and formatted. The final version may differ from this version.

The implications of the combination of approaches taken in this study are that in order to discover new potent PXR antagonists we should focus on molecules that possess a balanced hydrophobic and hydrogen bonding profile and conform more closely to the antagonist pharmacophore and the identified binding site 2 in terms of size. Previous studies have suggested that some microtubule stabilizing drugs displace the SMRT co-repressor interaction with human PXR to enhance activation (Mani et al., 2005). This would also suggest another pharmacophore to be aware of in developing antagonists to avoid inadvertently targeting this site. Although the azoles miconazole and oxiconazole have been shown not to act as PXR antagonists (Wang et al., 2007a), assessment of further azoles may be a starting point for extending this structure activity relationship. For example itraconazole, terconazole and voriconazole have greater than 90 % similarity to fluconazole when using ChemFinder (CambridgeSoft, Cambridge, MA). Assessment of antagonist activity of modified azoles is also currently being investigated.

In summary, this study has combined experimental data and computational approaches to suggest plausible differences between the binding sites for human PXR agonists and antagonists, using azoles, imidazoles, steroidal and other diverse molecules. We have demonstrated that a series of novel imidazoles behave as human PXR agonists (as predicted *a priori*) and lower affinity antagonists, the latter likely due to competitive inhibition of rifampicin binding in the LBD rather than at the AF-2 site. For the first time we suggest that azole PXR antagonists may require more hydrogen bonding interactions than agonists (or at least a different distribution of these molecular features). We also suggest computationally that the azole antagonists would partially mimic, displace or interfere with the co-activator SRC-1 binding at AF-2 or around this region on the outer

Molecular Pharmacology Fast Forward. Published on June 18, 2007 as DOI: 10.1124/mol.107.038398
This article has not been copyedited and formatted. The final version may differ from this version.

surface of PXR, explaining the in vitro and mutagenesis data. As both co-activators and co-repressors possibly bind the same AF-2 or other sites, this would suggest that development of antagonists provides a therapeutic option for control of PXR transcription of target genes. The identification of sulforaphane as the first naturally occurring PXR antagonist (Zhou et al., 2007), and more recently the phytoestrogen coumestrol (Wang et al., 2007b) may also indicate that a diverse array of molecules other than azoles, could bind the co-activator or other sites at low μM affinity. In the latter case, coumestrol possesses 2 hydroxyl groups as well as several other oxygen atoms that could serve as hydrogen bond acceptors, this molecule fits three features of the antagonist pharmacophore (both hydrogen bond acceptors and the ring aromatic feature) while omitting a hydrophobic feature (data not shown) suggesting it may bind the same site as the azoles. Interestingly, sulforaphane fits to the hydrogen bond acceptor features only (data not shown), providing weaker evidence that it could bind the external PXR surface. Computational methods are widely available that could explore these proposed antagonist binding sites with a more extensive and diverse array of molecules in a higher throughput fashion than possible *in vitro*, to enable the discovery of "drug-like" molecules. This will be achieved by database searching known drugs or commercially available libraries of molecules with the pharmacophores, or docking the molecules into the sites identified in this study, followed by *in vitro* verification. Such an approach has been successfully applied to define new transporter inhibitors and substrates (Chang et al., 2006; Ekins et al., 2005) and is currently ongoing for PXR.

Molecular Pharmacology Fast Forward. Published on June 18, 2007 as DOI: 10.1124/mol.107.038398
This article has not been copyedited and formatted. The final version may differ from this version.

ACKNOWLEDGMENTS

Dr. James Slama (University of Toledo, Toledo, OH) is gratefully acknowledged for synthesizing and providing the CDD imidazole compounds. We acknowledge Mr. John Ohrn and Dr. Shikha Varma (Accelrys, San Diego, CA) for their efforts in making Catalyst available to us. S.E. acknowledges Dr. Maggie A.Z. Hupcey for her moral support.

Molecular Pharmacology Fast Forward. Published on June 18, 2007 as DOI: 10.1124/mol.107.038398
This article has not been copyedited and formatted. The final version may differ from this version.

REFERENCES

Bachmann K, Patel H, Batayneh Z, Slama J, White D, Posey J, Ekins S, Gold D and Sambucetti L (2004) PXR and the regulation of apoA1 and HDL-cholesterol in rodents. *Pharmacol Res* **50**(3):237-246.

Bertilsson G, Heidrich J, Svensson K, Asman M, Jendeberg L, Sydow-Backman M, Ohlsson R, Postlind H, Blomquist P and Berkenstam A (1998) Identification of a human nuclear receptor defines a new signaling pathway for CYP3A induction. *Proc Natl Acad Sci U S A* **95**(21):12208-12213.

Bledsoe RK, Montana VG, Stanley TB, Delves CJ, Apolito CJ, McKee DD, Consler TG, Parks DJ, Stewart EL, Willson TM, Lambert MH, Moore JT, Pearce KH and Xu HE (2002) Crystal structure of the glucocorticoid receptor ligand binding domain reveals a novel mode of receptor dimerization and coactivator recognition. *Cell* **110**:93-105.

Blumberg B, Sabbagh W, Jr., Juguilon H, Bolado J, Jr., van Meter CM, Ong ES and Evans RM (1998) SXR, a novel steroid and xenobiotic-sensing nuclear receptor. *Genes Dev* **12**(20):3195-3205.

Chang C, Ekins S, Bahadduri P and Swaan PW (2006) Pharmacophore-based discovery of ligands for drug transporters. *Adv Drug Del Rev* **58**:1431-1450.

Clement OO and Mehl AT (2000) HipHop: Pharmacophore based on multiple common-feature alignments, in *Pharmacophore perception, development, and use in drug design* (Guner OF ed) pp 69-84, IUL, San Diego.

Coumol X, Diry M and Barouki R (2002) PXR-dependent induction of human CYP3A4 gene expression by organochlorine pesticides. *Biochem Pharmacol* **64**:1513-1519.

Cramer RD, Patterson DE and Bunce JD (1988) Comparative Molecular Field Analysis (CoMFA). 1. Effect of shape on binding of steroids to carrier proteins. *J Am Chem Soc* **110**:5959-5967.

Ding X and Staudinger JL (2005) Induction of drug metabolism by forskolin: the role of the pregnane X receptor and the protein kinase a signal transduction pathway. *J Pharmacol Exp Ther* **312**(2):849-856.

Drocourt L, Pascussi JM, Assenat E, Fabre JM, Maurel P and Vilarem MJ (2001) Calcium channel modulators of the dihydropyridine family are human pregnane X receptor activators and inducers of CYP3A, CYP2B, and CYP2C in human hepatocytes. *Drug Metab Dispos* **29**(10):1325-1331.

Dussault I, Lin M, Hollister K, Wang EH, Synold TW and Forman BM (2001) Peptide mimetic HIV protease inhibitors are ligands for the orphan receptor SXR. *J Biol Chem* **276**(36):33309-33312.

Ekins S, Andreyev S, Ryabov A, Kirillov E, Rakhmatulin EA, Sorokina S, Bugrim A and Nikolskaya T (2006) A Combined Approach to Drug Metabolism and Toxicity Assessment. *Drug Metab Dispos* **34**:495-503.

Ekins S and Erickson JA (2002) A pharmacophore for human pregnane-X-receptor ligands. *Drug Metab Dispos* **30**:96-99.

Ekins S, Johnston JS, Bahadduri P, D'Souzza VM, Ray A, Chang C and Swaan PW (2005) In Vitro And Pharmacophore Based Discovery Of Novel hPEPT1 Inhibitors. *Pharm Res* **22**:512-517.

Ekins S, Mankowski DC, Hoover DJ, Lawton MP, Treadway JL and Harwood HJ, Jr. (2007) Three-Dimensional Quantitative Structure-Activity Relationship Analysis of Human CYP51 Inhibitors. *Drug Metab Dispos* **35**(3):493-500.

Ekins S, Mirny L and Schuetz EG (2002) A ligand-based approach to understanding selectivity of nuclear hormone receptors PXR, CAR, FXR, LXRa and LXRb. *Pharm Res* **19**:1788-1800.

El-Sankary W, Gibson GG, Ayrton A and Plant N (2001) Use of a reporter gene assay to predict and rank the potency and efficiency of CYP3A4 inducers. *Drug Metab Dispos* **29**:1499-1504.

Goodwin B, Moore LB, Stoltz CM, McKee DD and Kliewer SA (2001) Regulation of the human CYP2B6 gene by the nuclear pregnane X receptor. *Mol Pharmacol* **60**(3):427-431.

Hamid R, Rotshteyn Y, Rabadi L, Parikh R and Bullock P (2004) Comparison of alamar blue and MTT assays for high through-put screening. *Toxicol In Vitro* **18**(5):703-710.

Huang H, Wang H, Sinz M, Zoeckler M, Staudinger J, Redinbo MR, Teotico DG, Locker J, Kalpana GV and Mani S (2007) Inhibition of drug metabolism by blocking the activation of nuclear receptors by ketoconazole. *Oncogene* **26**(2):258-268.

Jacobs MN (2004) In silico tools to aid risk assessment of endocrine disrupting chemicals. *Toxicology* **205**(1-2):43-53.

Jones G, Willett P, Glen RC, Leach AR and Taylor R (1997) Development and validation of a genetic algorithm for flexible docking. *J Mol Biol* **267**(3):727-748.

Kliewer SA, Moore JT, Wade L, Staudinger JL, Watson MA, Jones SA, McKee DD, Oliver BB, Willson TM, Zetterstrom RH, Perlmann T and Lehmann JM (1998) An orphan nuclear receptor activated by pregnanes defines a novel steroid signalling pathway. *Cell* **92**:73-82.

Krasowski MD, Yasuda K, Hagey LR and Schuetz EG (2005a) Evolution of the pregnane x receptor: adaptation to cross-species differences in biliary bile salts. *Mol Endocrinol* **19**(7):1720-1739.

Krasowski MD, Yasuda K, Hagey LR and Schuetz EG (2005b) Evolutionary selection across the nuclear hormone receptor superfamily with a focus on the NR1I subfamily (vitamin D, pregnane X, and constitutive androstane receptors). *Nucl Recept* **3**:2.

Leesnitzer LM, Parks DJ, Bledsoe RK, Cobb JE, Collins JL, Consler TG, Davis RG, Hull-Ryde EA, Lenhard JM, Patel L, Plunket KD, Shenk JL, Stimmel JB, Therapontos C, Willson TM and Blanchard SG (2002) Functional consequences of cysteine modification in the ligand binding sites of peroxisome proliferator activated receptors by GW9662. *Biochemistry* **41**:6640-6650.

Lehmann JM, McKee DD, Watson MA, Wilson TM, Moore JT and Kliewer SA (1998) The human orphan receptor PXR is activated by compounds that regulate CYP3A4 gene expressionand cause drug interactions. *J Clin Invest* **102**:1-8.

Lemaire G, de Sousa G and Rahmani R (2004) A PXR reporter gene assay in a stable cell culture system: CYP3A4 and CYP2B6 induction by pesticides. *Biochem Pharmacol* **68**(12):2347-2358.

Luo G, Cunningham M, kim S, Burn T, Lin J, Sinz M, Hamilton GA, Rizzo C, Jolley S, Gilbert D, Downey A, Mudra D, Graham R, Carroll K, Xie J, Madan A, Parkinson A, Christ D, Selling B, LeCluyse EL and Gan L-S (2002) CYP3A4 induction by drugs: correlation between a pregnane X receptor reporter gene assay and CYP3A4 expression in human hepatocytes. *Drug Metab Dispos* **30**:795-804.

Mani S, Huang H, Sundarababu S, Liu W, Kalpana G, Smith AB and Horwitz SB (2005) Activation of the steroid and xenobiotic receptor (human pregnane X receptor) by nontaxane microtubule-stabilizing agents. *Clin Cancer Res* **11**(17):6359-6369.

Masuyama H, Hiramatsu Y, Kunitomi M, Kudo T and MacDonald PN (2000) Endocrine disrupting chemicals, phthalic acid and nonylphenol, activate Pregnane X receptor-mediated transcription. *Mol Endocrinol* **14**(3):421-428.

Masuyama H, Inoshita H, Hiramatsu Y and Kudo T (2002) Ligands have various potential effects on the degradation of pregnane X receptor by proteasome. *Endocrinology* **143**(1):55-61.

Matsuura K, Yoshioka S, Tosha T, Hori H, Ishimori K, Kitagawa T, Morishima I, Kagawa N and Waterman MR (2005) Structural diversities of active site in clinical azole-bound forms between sterol 14alpha-demethylases (CYP51s) from human and Mycobacterium tuberculosis. *J Biol Chem* **280**(10):9088-9096.

Moore JT and Kliewer SA (2000) Use of the nuclear receptor PXR to predict drug interactions. *Toxicology* **153**(1-3):1-10.

Moore LB, Goodwin B, Jones SA, Wisely GB, Serabjit-Singh CJ, Willson TM, Collins JL and Kliewer SA (2000) St John's Wort induces hepatic drug metabolism

through activation of the pregnane X receptor. *Proc Natl Acad Sci USA* **97**:7500-7502.

Mu Y, Stephenson CR, Kendall C, Saini SP, Toma D, Ren S, Cai H, Strom SC, Day BW, Wipf P and Xie W (2005) A pregnane X receptor agonist with unique species-dependent stereoselectivity and its implications in drug development. *Mol Pharmacol* **68**(2):403-413.

Mu Y, Zhang J, Zhang S, Zhou HH, Toma D, Ren S, Huang L, Yaramus M, Baum A, Venkataramanan R and Xie W (2006) Traditional Chinese medicines Wu Wei Zi (Schisandra chinensis Baill) and Gan Cao (Glycyrrhiza uralensis Fisch) activate pregnane X receptor and increase warfarin clearance in rats. *J Pharmacol Exp Ther* **316**(3):1369-1377.

Ruhl R (2005) Induction of PXR-mediated metabolism by beta-carotene. *Biochim Biophys Acta* **1740**(2):162-169.

Ruhl R, Sczech R, Landes N, Pfluger P, Kluth D and Schweigert FJ (2004) Carotenoids and their metabolites are naturally occurring activators of gene expression via the pregnane X receptor. *Eur J Nutr* **43**(6):336-343.

Schuetz E and Strom S (2001) Promiscous regulator of xenobiotic removal. *Nature Medicine* **7**:536-537.

Schuster D, Laggner C, Steindl TM, Palusczak A, Hartmann RW and Langer T (2006) Pharmacophore modeling and in silico screening for new P450 19 (aromatase) inhibitors. *J Chem Inf Model* **46**(3):1301-1311.

Sinz M, Kim S, Zhu Z, Chen T, Anthony M, Dickinson K and Rodrigues AD (2006) Evaluation of 170 xenobiotics as transactivators of human pregnane X receptor

(hPXR) and correlation to known CYP3A4 drug interactions. *Curr Drug Metab* **7**(4):375-388.

Sonoda J, Chong LW, Downes M, Barish GD, Coulter S, Liddle C, Lee CH and Evans RM (2005) Pregnane X receptor prevents hepatorenal toxicity from cholesterol metabolites. *Proc Natl Acad Sci U S A* **102**(6):2198-2203.

Staudinger J, Liu Y, Madan A, Habeebu S and Klaassen CD (2001a) Coordinate regulation of xenobiotic and bile acid homeostasis by pregnane X receptor. *Drug Metab Dispos* **29**(11):1467-1472.

Staudinger JL, Goodwin B, Jones SA, Hawkins-Brown D, MacKenzie KI, LaTour A, Liu Y, Klaassen CD, Brown KK, Reinhard J, Willson TM, Koller BH and Kliewer SA (2001b) The nuclear receptor PXR is a lithocholic acid sensor that protects against liver toxicity. *Proc Natl Acad Sci U S A* **98**(6):3369-3374.

Synold TW, Dussault I and Forman BM (2001) The orphan nuclear receptor SXR coordinately regulates drug metabolism and efflux. *Nature Medicine* **7**:584-590.

Tabb MM, Kholodovych V, Grun F, Zhou C, Welsh WJ and Blumberg B (2004) Highly chlorinated PCBs inhibit the human xenobiotic response mediated by the steroid and xenobiotic receptor (SXR). *Environ Health Perspect* **112**(2):163-169.

Takeshita A, Inagaki K, Igarashi-Migitaka J, Ozawa Y and Koibuchi N (2006) The endocrine disrupting chemical, diethylhexyl phthalate, activates MDR1 gene expression in human colon cancer LS174T cells. *J Endocrinol* **190**(3):897-902.

Takeshita A, Koibuchi N, Oka J, Taguchi M, Shishiba Y and Ozawa Y (2001) Bisphenol-A, an environmental estrogen, activates the human orphan nuclear receptor,

steroid and xenobiotic receptor-mediated transcription. *Eur J Endocrinol* **145**(4):513-517.

Takeshita A, Taguchi M, Koibuchi N and Ozawa Y (2002) Putative role of the orphan nuclear receptor SXR (steroid and xenobiotic receptor) in the mechanism of CYP3A4 inhibition by xenobiotics. *J Biol Chem* **277**(36):32453-32458.

Ung CY, Li H, Yap CW and Chen YZ (2007) In silico prediction of pregnane X receptor activators by machine learning approaches. *Mol Pharmacol* **71**(1):158-168.

Wang CY, Li CW, Chen JD and Welsh WJ (2006) Structural model reveals key interactions in the assembly of the pregnane X receptor/corepressor complex. *Mol Pharmacol* **69**(5):1513-1517.

Wang H, Huang H, Li H, Teotico DG, Sinz M, Baker SD, Staudinger J, Kalpana G, Redinbo MR and Mani S (2007a) Activated PXR is a target for ketoconazole and its analogs. *Clin Cancer Res* **13**(8):2488-2495.

Wang H, Li H, Moore LB, Maglich JM, Goodwin B, Ittopp ORR, Wisely B, Creech K, Parks DJ, Collins JL, Willson TM, Kalpana GV, Xie W, Redinbo MR, Moore JT and Mani S (2007b) The phytoestrogen coumestrol is a naturally-occuring antagonist of the pregnane X receptor (PXR). *Mol Endocrinol* **Submitted**.

Warnmark A, Treuter E, Gustafsson JA, Hubbard RE, Brzozowski AM and Pike AC (2002) Interaction of transcriptional intermediary factor 2 nuclear receptor box peptides with the coactivator binding site of estrogen receptor alpha. *J Biol Chem* **277**(24):21862-21868.

Watkins RE, Davis-Searles PR, Lambert MH and Redinbo MR (2003a) Coactivator binding promotes the specific interaction between ligand and the pregnane X receptor. *J Mol Biol* **331**:815-828.

Watkins RE, Maglich JM, Moore LB, Wisely GB, Noble SM, Davis-Searles PR, Lambert MH, Kliewer SA and Redinbo MR (2003b) 2.1A crystal structure of human PXR in complex with the St John's Wort compound hyperforin. *Biochemistry* **42**:1430-1438.

Watkins RE, Noble SM and Redinbo MR (2002) Structural insights into the promiscuity and function of the human pregnane X receptor. *Curr Opin Drug Discov Devel* **5**(1):150-158.

Watkins RE, Wisely GB, Moore LB, Collins JL, Lambert MH, Williams SP, Willson TM, Kliewer SA and Redinbo MR (2001) The human nuclear xenobiotic receptor PXR: structural determinants of directed promiscuity. *Science* **292**:2329-2333.

Waxman DJ (1999) P450 gene induction by structurally diverse xenochemicals: central role of nuclear receptors CAR, PXR, and PPAR. *Arch Biochem Biophys* **369**(1):11-23.

Xue Y, Chao E, Zuercher WJ, Willson TM, Collins JL and Redinbo MR (2007a) Crystal structure of the PXR-T1317 complex provides a scaffold to examine the potential for receptor antagonism. *Bioorg Med Chem* **15(**5):2156-2166.

Xue Y, Moore LB, Orans J, Peng L, Bencharit S, Kliewer SA and Redinbo MR (2007b) Crystal structure of the pregnane X receptor-estradiol complex provides insights into endobiotic recognition. *Mol Endocrinol* **21**(5):1028-1038.

Zhou C, Poulton EJ, Grun F, Bammler TK, Blumberg B, Thummel KE and Eaton DL (2007) The dietary isothiocyanate sulforaphane is an antagonist of the human steroid and xenobiotic nuclear receptor. *Mol Pharmacol* **71**(1):220-229.

Zhou C, Tabb MM, Sadatrafiei A, Grun F and Blumberg B (2004) Tocotrienols activate the steroid and xenobiotic receptor, SXR, and selectively regulate expression of its target genes. *Drug Metab Dispos* **32**(10):1075-1082.

Zhu Z, Kim S, Chen T, Lin JH, Bell A, Bryson J, Dubaquie Y, Yan N, Yanchunas J, Xie D, Stoffel R, Sinz M and Dickinson K (2004) Correlation of high-throughput pregnane X receptor (PXR) transactivation and binding assays. *J Biomol Screen* **9**(6):533-540.

Molecular Pharmacology Fast Forward. Published on June 18, 2007 as DOI: 10.1124/mol.107.038398
This article has not been copyedited and formatted. The final version may differ from this version.

FOOTNOTES PAGE

a) Unnumbered footnotes

Equal contribution (SE, CC, SM)

b) M.D.K. is supported by K08-GM074238 from the National Institutes of Health and a Competitive Medical Research Fund (CMRF) grant from the University of Pittsburgh Medical Center. M.I. received support from a University of Pittsburgh Pathology Post-doctoral Research Training Program. N.A, V. K., and W.J.W. gratefully acknowledge the support for this work provided by the USEPA-funded Environmental Bioinformatics and Computational Toxicology Center (ebCTC), under STAR Grant number GAD R 832721-010.

c) Send reprint requests to:

Sean Ekins, D.Sc., ACT LLC, 601 Runnymede Avenue, Jenkintown, PA 19046. Email ekinssean@yahoo.com

d) Numbered footnotes

ACT LLC, 601 Runnymede Avenue, Jenkintown, PA 19046 (SE)

Department of Pharmaceutical Sciences, University of Maryland, 20 Penn Street, Baltimore, MD 21201 (SE, CC, PWS)

Present address: Pharmacokinetics, Dynamics, and Metabolism, Pfizer PGRD, Ann Arbor, MI 48105 (CC)

Albert Einstein Cancer Center, Albert Einstein College of Medicine, Bronx, NY 10461 (SM)

Department of Medicine, Albert Einstein College of Medicine, Bronx, NY 10461 (SM)

Department of Pathology, University of Pittsburgh Medical Center, Pittsburgh, PA 15261, USA (MDK, EJR, MI)

Department of Pharmacology, University of Medicine and Dentistry of New Jersey, Robert Wood Johnson Medical School, 675 Hoes Lane, Piscataway, NJ 08854, USA. (VK, NA, WJW)

Bristol-Myers Squibb Company, Research Parkway, Wallingford, CT 06492 USA (MS)

Department of Pharmacology, The University of Toledo, 2801 W. Bancroft St., Toledo, OH 43606, USA.(RP, KB)

Current address: Sun Pharmaceutical Industries Inc., Bryan, OH 43506, USA.(RP)

Molecular Pharmacology Fast Forward. Published on June 18, 2007 as DOI: 10.1124/mol.107.038398
This article has not been copyedited and formatted. The final version may differ from this version.

FIGURE LEGENDS

Figure 1. Structures of selected PXR agonists and antagonists. A. Imidazoles (Bachmann et al., 2004), B. Steroidal molecules and hyperforin (Sinz et al., 2006), C. 2,2´,3,3´,4,4´,6,6´-OctaChloroBiphenyl (Tabb et al., 2004) and D. Azoles (Wang et al., 2007a).

Figure 2. PXR agonist models A. Azole PXR agonist HIPHOP pharmacophore, showing CDD 3501 aligned to ring aromatic features (brown) and a hydrogen bond acceptor (green). B. Azole PXR agonist CoMFA model with coefficient contour map aligned with all training set compounds. C. Steroidal PXR pharmacophore: The pharmacophore possessed one hydrogen bond acceptor (green) and 4 hydrophobes (cyan). Aligned are the two most active compounds 5α-Androstan-3β-ol (red) and lithocholic acid acetate (gray) showing the mapping to these features. D. Diverse PXR agonist Hypogen pharmacophore showing hyperforin aligned to hydrophobes (cyan), Hydrogen bond acceptor (green) and hydrogen bond donor (purple) features.

Figure 3. PXR antagonist models A. Biphenol PXR antagonist CoMFA model showing coefficient contour map aligned with the most active biphenyl 2,2´,3,3´,4,4´,6,6´-OctaChloroBiphenyl.

B. Imidazole PXR antagonist HIPHOP pharmacophore. A. Enilconazole (red), ketoconazole (purple) and fluconazole (cyan) mapped to hydrogen bond acceptors (green), hydrophobic (cyan) and ring aromatic features (orange).

Molecular Pharmacology Fast Forward. Published on June 18, 2007 as DOI: 10.1124/mol.107.038398
This article has not been copyedited and formatted. The final version may differ from this version.

Figure 4. Docking of azoles in PXR 1NRL using GOLD. A. All azole antagonists align well in the binding site 2 and the azole ring of ketoconazole is exposed to solvent, B. Ketoconazole with van der Waals surface showing the fit into the binding pocket.

Molecular Pharmacology Fast Forward. Published on June 18, 2007 as DOI: 10.1124/mol.107.038398
This article has not been copyedited and formatted. The final version may differ from this version.

Table 1. Imidazole agonists with experimental PXR data and predictions. Side-by-side comparison of E_{max} and EC_{50} values were obtained utilizing the two dose response curve modeling equations and the experimental E_{max} values. E_{max} refers to the maximum increase in fold-induction obtained when DPX-2 cells were treated with PXR agonists, over cells treated with the negative control, 0.1% DMSO. The experimental E_{max} is the highest observed fold induction for each compound. The fold induction results were corrected for cell viability and represent the mean of 3 or 4 determinations. For further experimental details refer to Materials and Methods.

Compound		**Via Simple E_{max} Model**		**Via Hill's Model**		**Experimental E_{max}**	
	Prediction from (Bachmann et al., 2004)(μM)	**E_{max}**	**EC_{50} (μM)**	**E_{max}**	**EC_{50} (μM)**	**Concentration (μM)**	**E_{max}**
Rifampicin	-	33.9	4.1	35	4.7	20	31
Mifepristone	-	16.2	3.1	16.5	4	10	15.3
Androstenol	-	9.9	1.9	9	1.8	10	8.8
CDD 3501	-	22.4	2.3	19	1.8	10	20.3
CDD 3508	-	36	4.1	34	3.9	10	29.7
CDD 3530	-	26.6	3.6	22.5	3.1	10	24
CDD 3532	-	20.6	1.5	20.9	2	20	20.2
Clotrimazole	-	16	0.8	15	0.8	20	16.2

Molecular Pharmacology Fast Forward. Published on June 18, 2007 as DOI: 10.1124/mol.107.038398
This article has not been copyedited and formatted. The final version may differ from this version.

CDD 3536	-	24	2.4	24.2	2.5	20	22.2
CDD 3538	9.6	30.2	1.3	27.8	1.1	10	30.9
CDD 3540	25	31.5	2.3	26.9	1.7	10	32.7
CDD 3543	3.4	25.7	1.4	25.1	1.4	10	25.7

Molecular Pharmacology Fast Forward. Published on June 18, 2007 as DOI: 10.1124/mol.107.038398
This article has not been copyedited and formatted. The final version may differ from this version.

Table 2. Imidazoles with PXR transactivation agonist and antagonist data from HepG2 cells. The luciferase based reporter assay was performed using HepG2 cells as described previously (Zhu et al., 2004) using an 11 point dose response curve from 2.5 - 50 μM. Maximum activation observed = % of rifampcin response at 10 μM. For further experimental details refer to Materials and Methods.

Compound	Luciferase-DMSO (agonist mode)		Luciferase-Rifampicin (antagonist mode)	
	EC_{50},(μM)	Maximum activation observed (%)	EC_{50},(μM)	Maximum activation observed (%)
CDD3508	4.4	73	23.9	108
CDD3530	1.5	70	14.3	110
CDD3532	1.3	81	14.4	110
CDD3538	1.4	92	18.4	108
CDD3540	1.9	56	15.8	110
Clotrimazole	1.1	96	16.7	107

Molecular Pharmacology Fast Forward. Published on June 18, 2007 as DOI: 10.1124/mol.107.038398
This article has not been copyedited and formatted. The final version may differ from this version.

Table 3. Concentration response data for steroidal ligands activating human PXR in HepG2 cells. PXR activation in the HepG2 human liver cell line was determined by a luciferase-based reporter assay as previously described (Krasowski et al., 2005b). Each drug concentration was performed at least in quadruplicate and repeated in separate experiments for a total of at least three times. Data are expressed as mean ± SD. For further experimental details refer to Materials and Methods.

Compound Name	EC_{50} (μM)	Efficacy
17β-dihydroandrosterone	4.15 ± 0.2	0.68
Androstanol	6.27 ± 0.3	0.5
Dihydrotestosterone	11.4 ± 0.5	0.39
Etiocholanolone	5.7 ± 0.6	0.54
5β-Cholan-3α,7α,12α,24-tetrol	> 100	0
Taurochenodeoxycholic acid *	104 ± 8	0.5
Deoxycholic acid *	50.2 ± 4.5	0.19
Lithocholic acid *	10 ± 0.1	0.15
7-Ketolithocholic acid *	21.5 ± 1.4	0.58
12-Ketolithocholic acid *	31.3 ± 5.8	0.86
ω-Muricholic acid *	> 100	0
Taurocholic acid *	> 100	0
Cholesterol	> 100	0
Estradiol	16 ± 0.1	0.34

Molecular Pharmacology Fast Forward. Published on June 18, 2007 as DOI: 10.1124/mol.107.038398
This article has not been copyedited and formatted. The final version may differ from this version.

Estrone	37.9 ± 3.3	0.47
Estriol	> 100	0
5β-Pregnane-3,20-dione	2.6 ± 0.2	0.97
17-Hydroxyprogesterone	17.7 ± 2.3	0.7
Petromyzonol *	> 100	0
Allocholic acid *	> 100	0
PCN	> 100	0
Cortolone	44.7 ± 7.4	0.72
Estetrol	2.14 ± 0.2	0.29
Epitestosterone sulfate	3.39 ± 0.7	0.67
5β-Pregnan-3α,20β,diol	3.81 ± 0.3	0.49
5α-Androstan-3β-ol	0.8 ± 0.01	0.43
16,(5α)-Androsten-3β-ol	4.77 ± 1.0	1.01
5β-Androstan-3α-ol	1.41 ± 0.1	1.12
Tauro-β-muricholic acid *	> 100	0
Lithocholic acid acetate *	1.2 ± 0.2	0.54

* previously published (Krasowski et al., 2005a)

Molecular Pharmacology Fast Forward. Published on June 18, 2007 as DOI: 10.1124/mol.107.038398
This article has not been copyedited and formatted. The final version may differ from this version.

Figure 1
A.

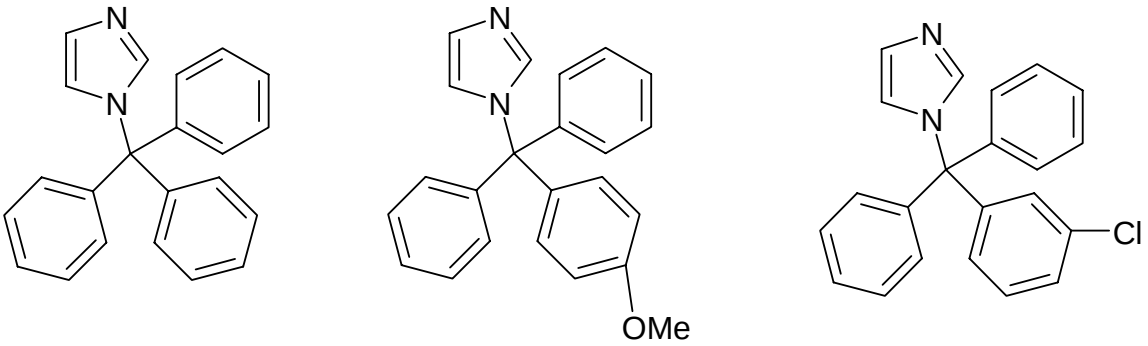

CDD3501 CDD3508 CDD3530

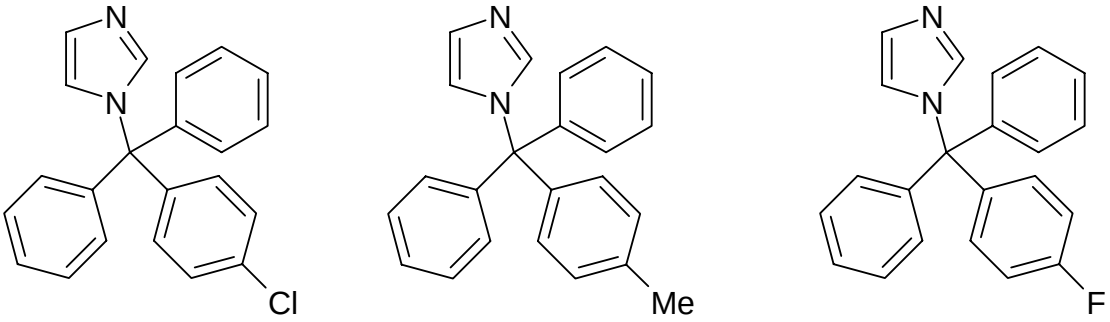

CDD3532 CDD3536 CDD3538

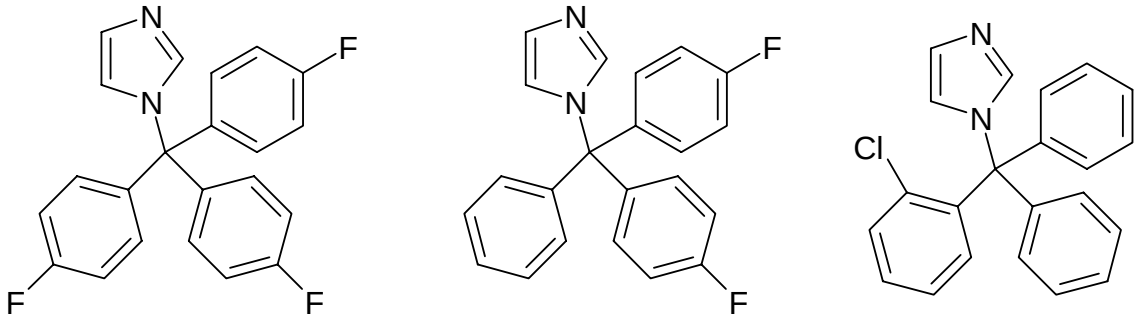

CDD3540 CDD3543 Clotrimazole

Molecular Pharmacology Fast Forward. Published on June 18, 2007 as DOI: 10.1124/mol.107.038398
This article has not been copyedited and formatted. The final version may differ from this version.

Figure 1
B.

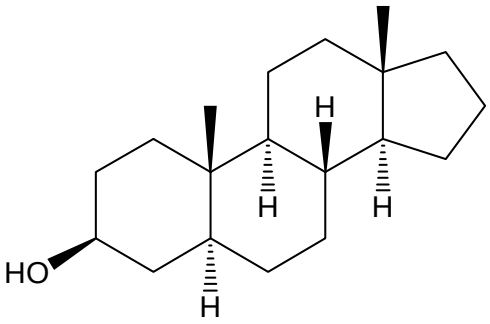

5a-Androstan-3b-ol

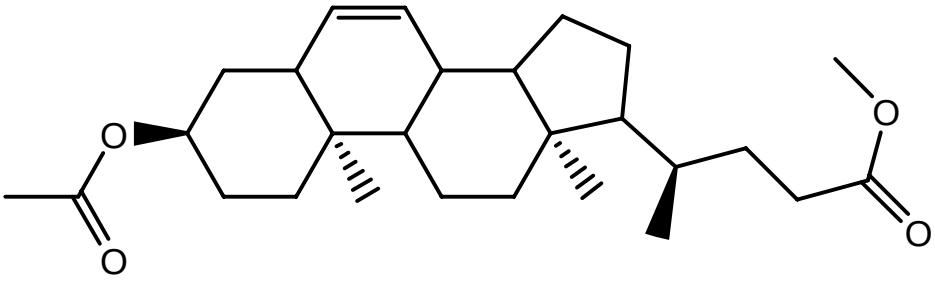

lithocholic acid acetate

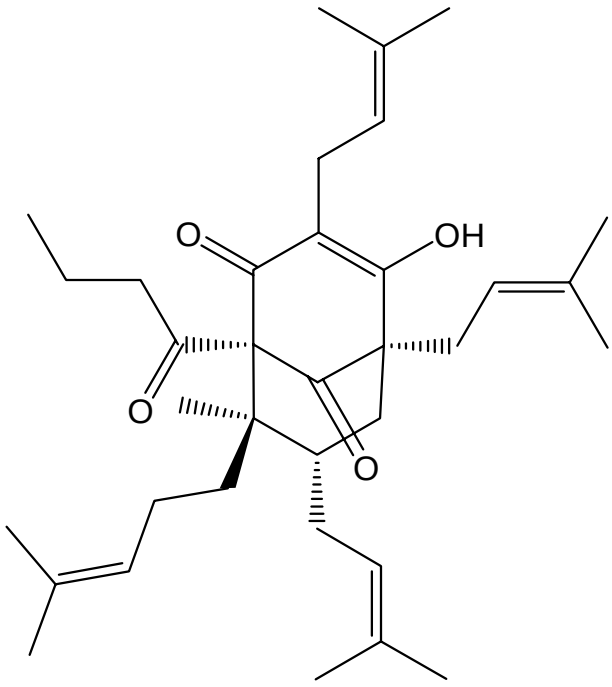

hyperforin

Molecular Pharmacology Fast Forward. Published on June 18, 2007 as DOI: 10.1124/mol.107.038398
This article has not been copyedited and formatted. The final version may differ from this version.

Figure 1
C.

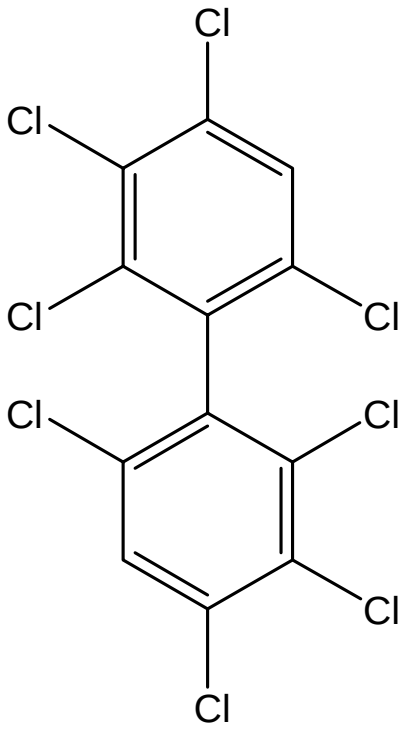

2,2´,3,3´,4,4´,6,6´-OctaChloroBiphenyl

Molecular Pharmacology Fast Forward. Published on June 18, 2007 as DOI: 10.1124/mol.107.038398
This article has not been copyedited and formatted. The final version may differ from this version.

Figure 1
D.

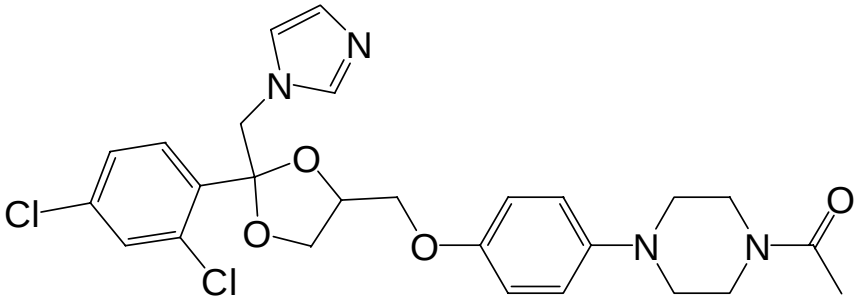

Ketoconazole

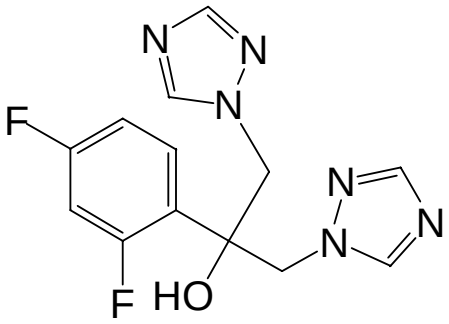

Fluconazole

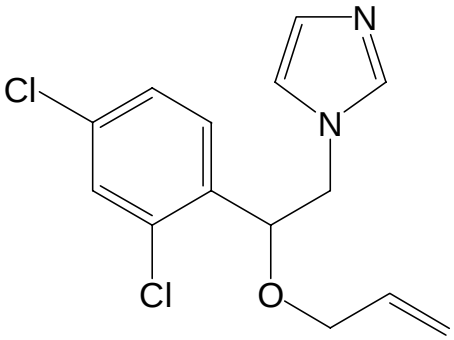

Enilconazole

Fig 2a

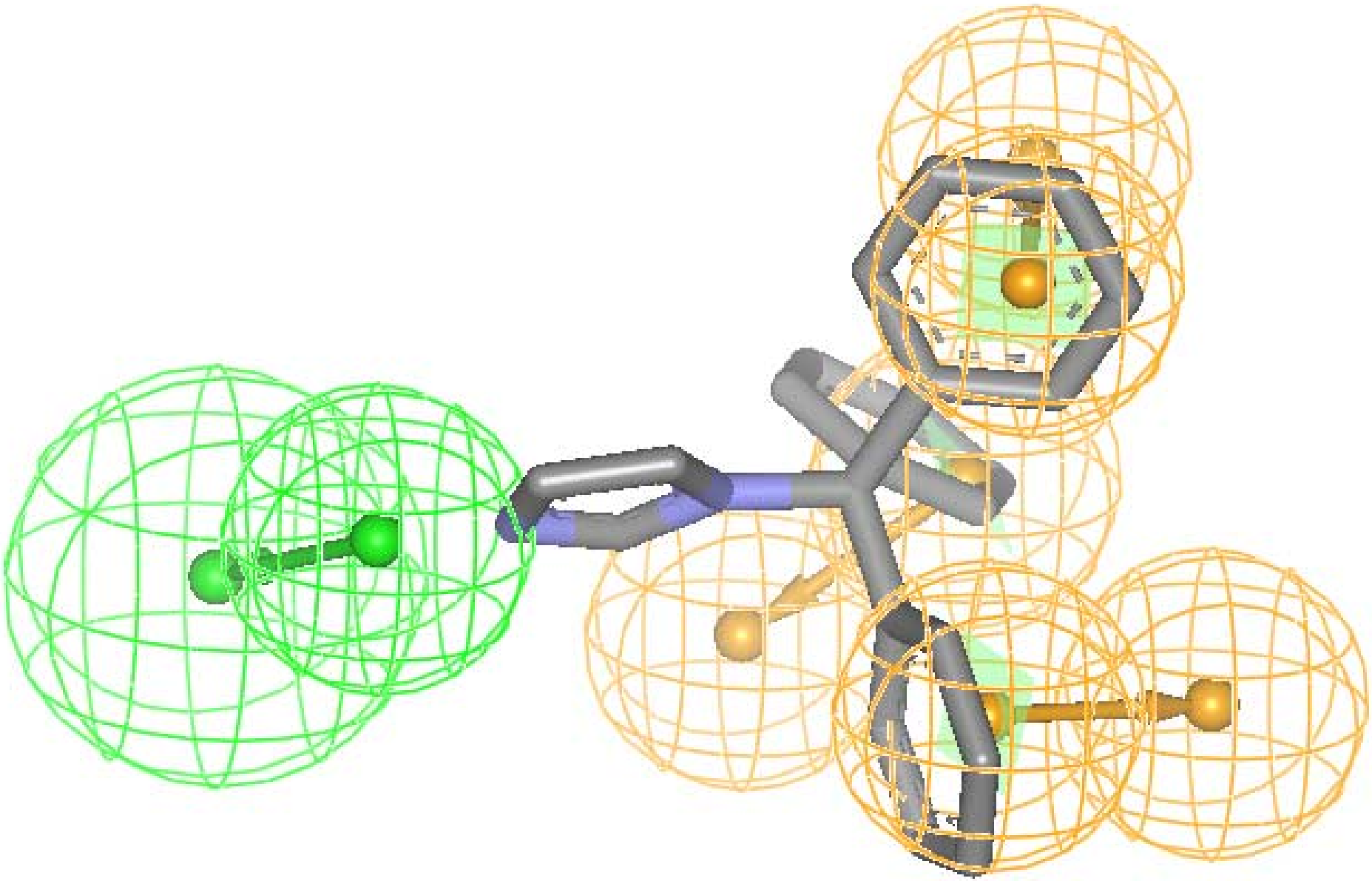

Molecular Pharmacology Fast Forward. Published on June 18, 2007 as DOI: 10.1124/mol.107.038398
This article has not been copyedited and formatted. The final version may differ from this version.

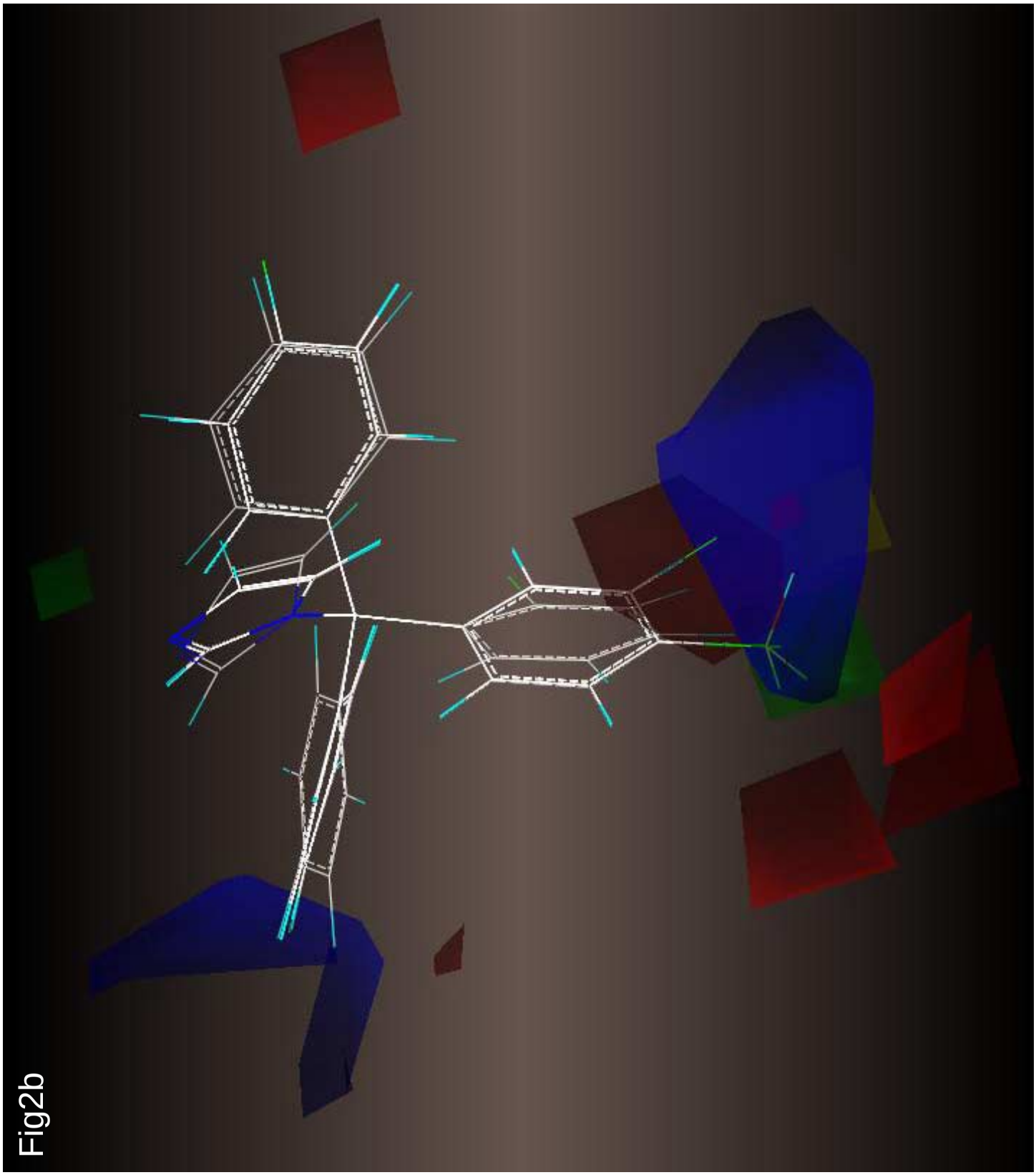

Fig2b

Molecular Pharmacology Fast Forward. Published on June 18, 2007 as DOI: 10.1124/mol.107.038398
This article has not been copyedited and formatted. The final version may differ from this version.

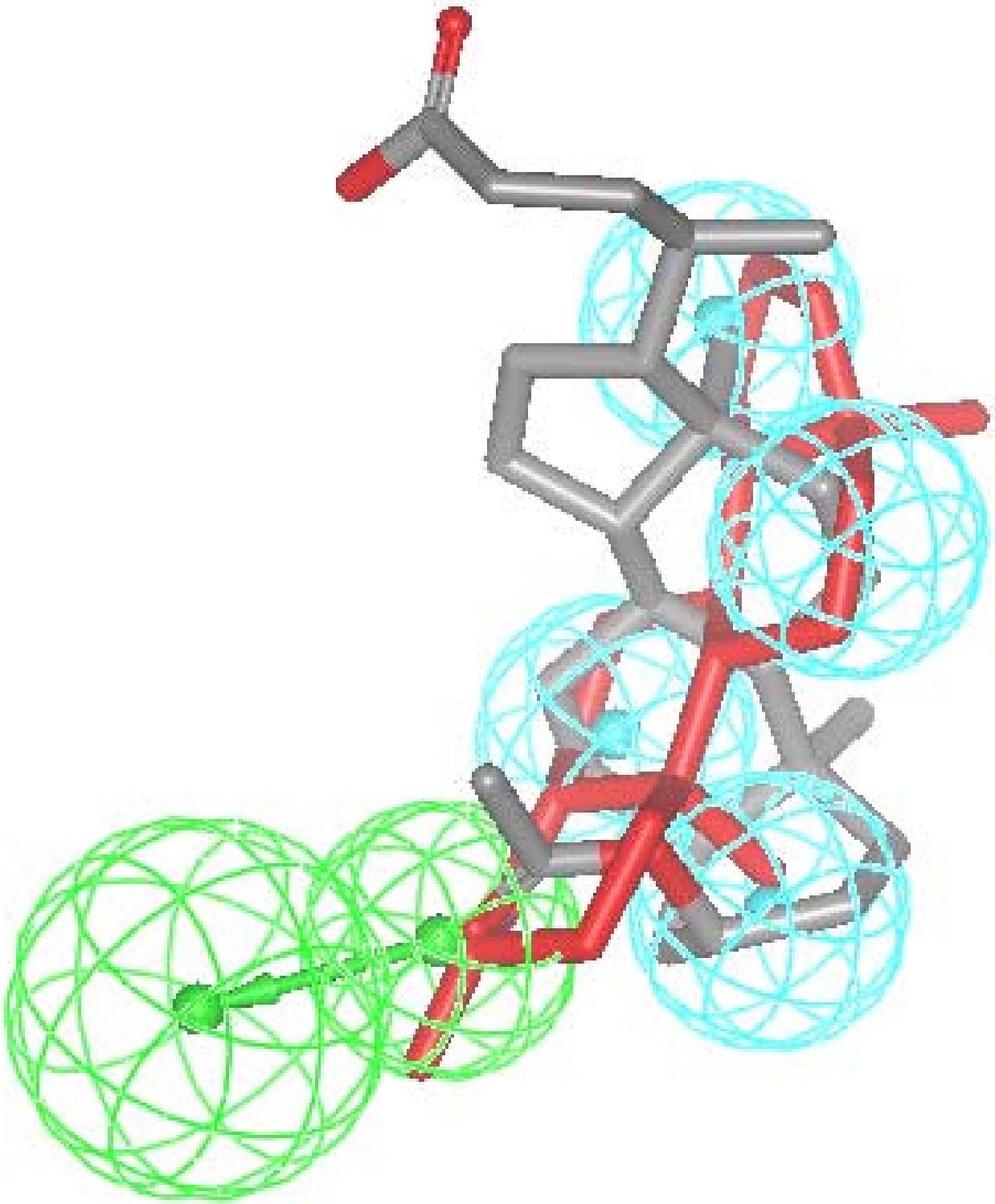

Fig2c

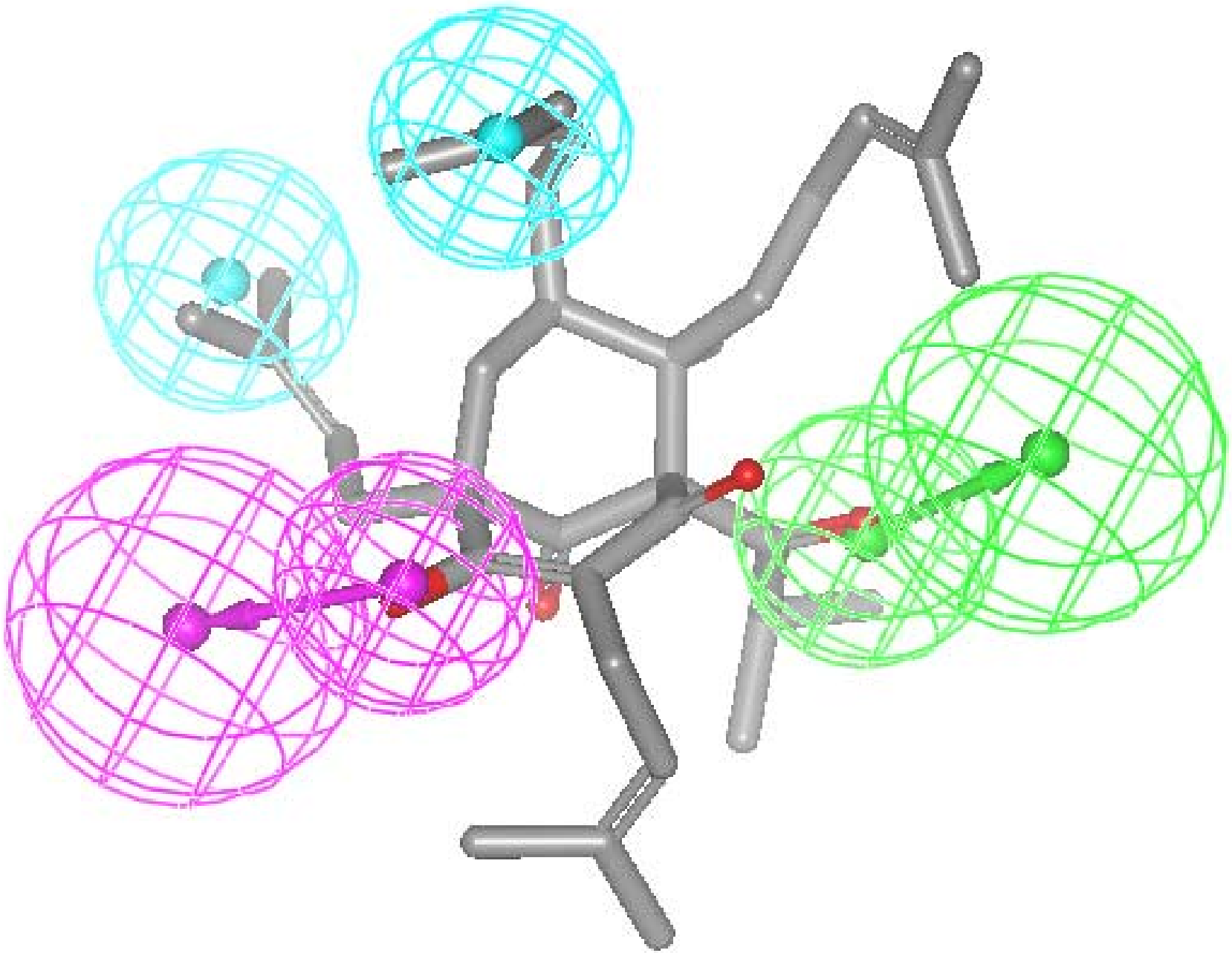

Fig2d

Fig3a

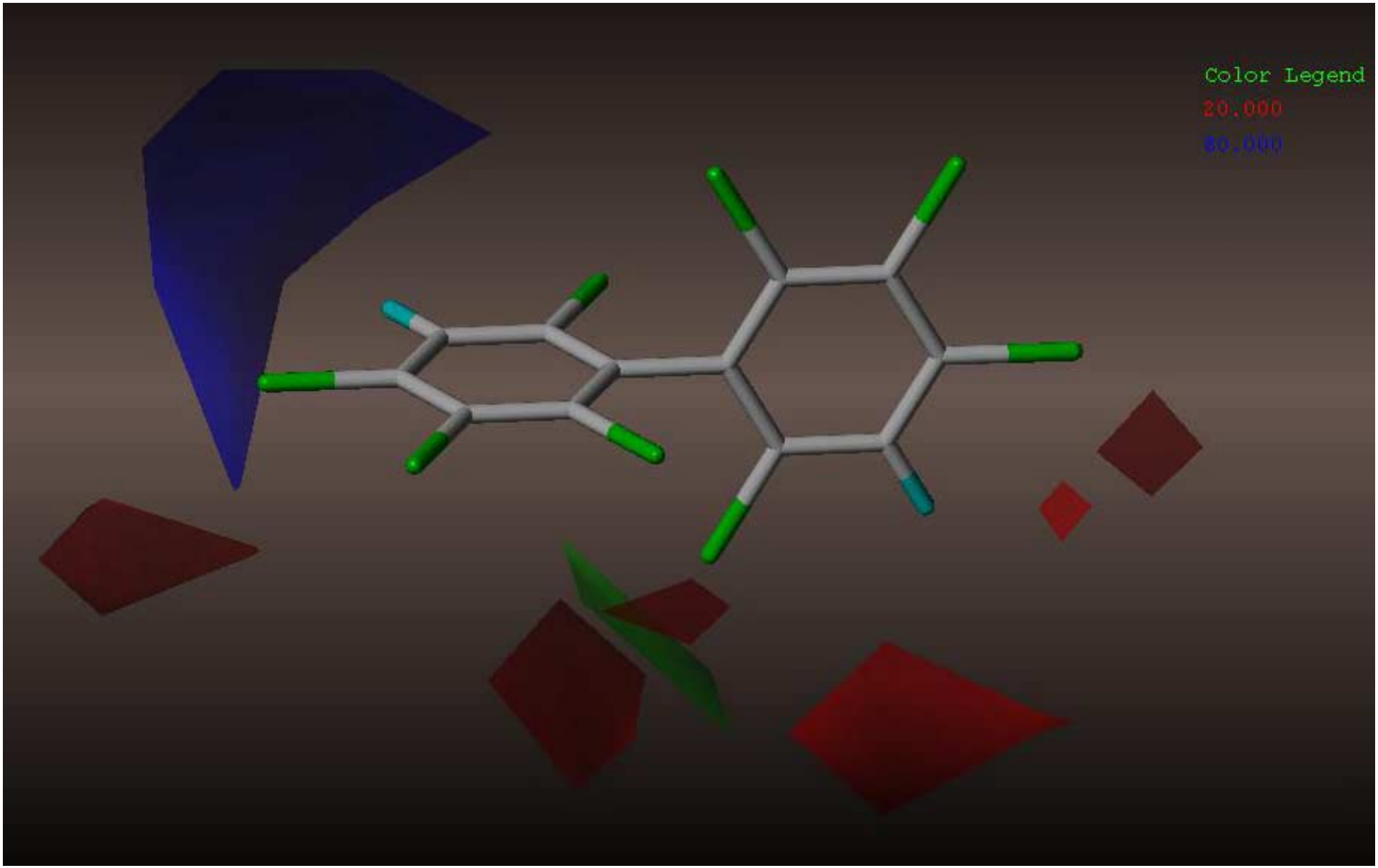

Fig3b

Fig4a

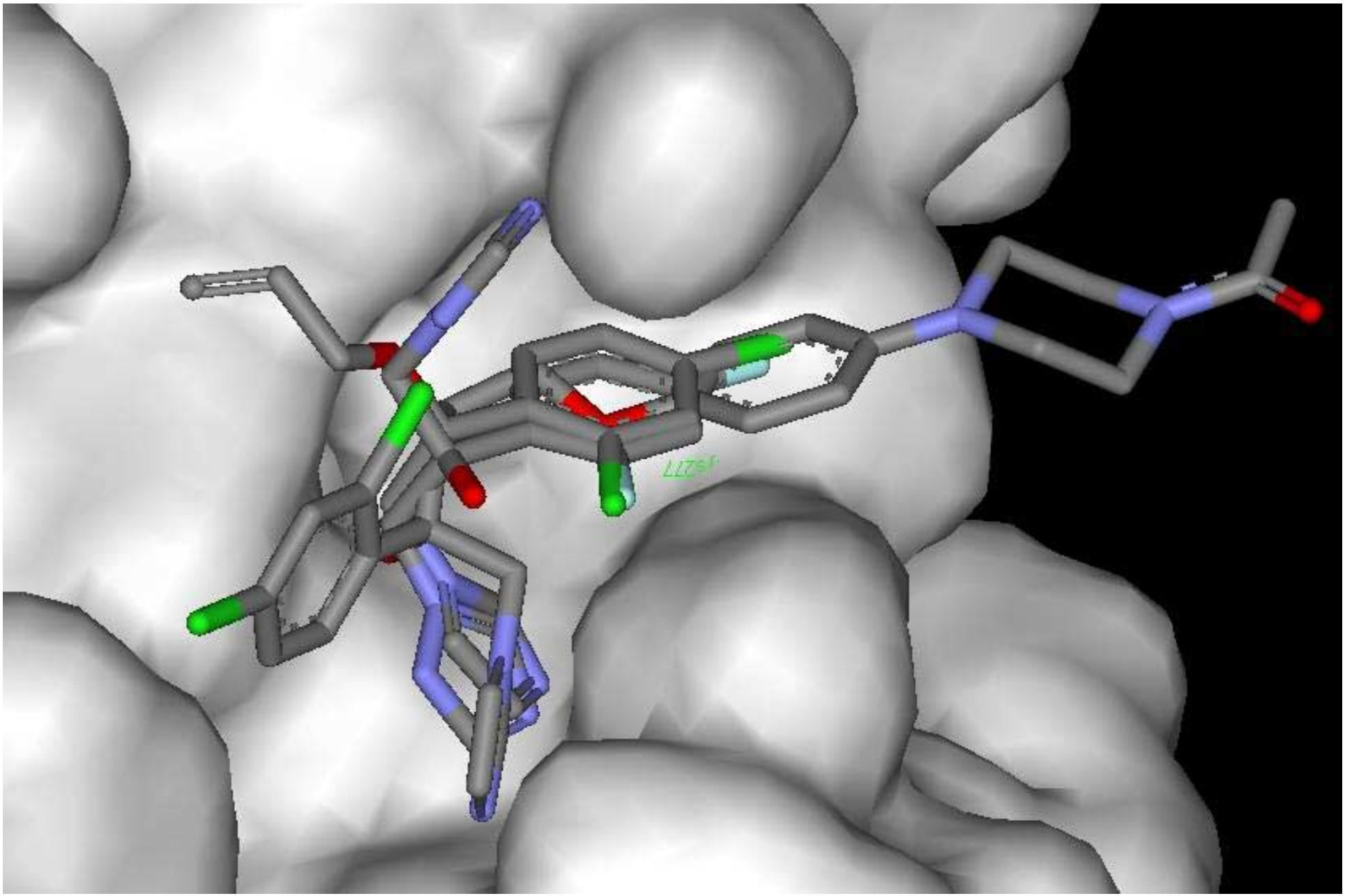

Fig 4B